Quaternary Science Reviews 308 (2023) 108068

Contents lists available at ScienceDirect

Quaternary Science Reviews

journal homepage: www.elsevier.com/locate/quascirev

Ice-ocean interactions at the Northeast Greenland Ice stream (NEGIS) over the past 11,000 years

J.M. Lloyd [a, *], S. Ribeiro [b], K. Weckström [b, c], L. Callard [d], C. Ó Cofaigh [a], M.J. Leng [e], P. Gulliver [f], D.H. Roberts [a]

[a] Department of Geography, Durham University, Durham, DH1 3LE, UK
[b] Glaciology and Climate Department, Geological Survey of Denmark and Greenland, 1350, Copenhagen, Denmark
[c] Ecosystems and Environment Research Programme (ECRU), Faculty of Biological and Environmental Sciences, University of Helsinki, P.O.Box 65 (Vikinkaari 1), 00014, Finland
[d] School of Geography, Politics and Sociology, Newcastle University, Newcastle Upon Tyne, NE1 7RU, UK
[e] National Environmental Isotope Facility, British Geological Survey, Keyworth NG12 5GG, UK, School of Biosciences, University of Nottingham, Sutton Bonington, LE12 5RD, UK
[f] NERC Radiocarbon Facility, East Kilbridge, G75 0QF, UK

ARTICLE INFO

Article history:
Received 17 November 2022
Received in revised form
14 March 2023
Accepted 25 March 2023
Available online xxx

Handling Editor: I Hendy

Keywords:
Holocene
Paleoceanography
Greenland
Foraminifera
Dinocysts
Sedimentology
Marine cores

ABSTRACT

Recent observations have identified increased mass loss from Greenland marine-terminating outlet glaciers (MTOG) with implications for global sea-level rise and wider ocean circulation. The flow of Atlantic-sourced waters to the Greenland margin is thought to be a major control on MTOG behaviour. Investigation of longer-term records of the role of Atlantic-sourced waters on MOTG dynamics are needed to improve understanding of potential future trends in MTOG behaviour. Here we present a multi-proxy study (benthic and planktic foraminifera, dinoflagellate cysts, diatoms, stable isotopes, sea ice biomarkers and sedimentological analyses) from core PS100-198 on the northeast Greenland shelf to investigate the interaction between the Northeast Greenland Ice Stream (NEGIS) and ocean circulation through the Holocene. Proximal glaciomarine conditions at the base of the core indicate deglaciation before 10.9 ka cal BP with the relatively warm Atlantic Water present through advection of the Return Atlantic Current (RAC) across the shelf. The advection of RAC increased through the early Holocene reaching peak subsurface warmth from 8 to 9 ka cal BP. Surface conditions at this time were characterised by heavy sea-ice cover. During the mid-to late Holocene (*c.* 7–2 ka cal BP) advection of RAC weakened with cooler subsurface waters, but with an amelioration of surface conditions characterised by seasonal sea ice. From *c.* 2 ka cal BP, during the late Holocene, surface conditions continued to improve with continued seasonal sea-ice cover while subsurface proxies record an increase in RAC advection. The last *c.* 100 years represent the most ameliorated surface conditions through the Holocene and with subsurface conditions as warm as the early Holocene peak. This coincided with the final break up of ice within 79N fjord and retreat of NEGIS to the Holocene minimum position. Current conditions, therefore, suggest the present-day ice shelf within 79N fjord is most likely susceptible to collapse in the near future. This study highlights the critical influence of Atlantic-sourced waters on the dynamics of major Greenland MTOGs.

1. Introduction

Over recent decades, anthropogenic climate change has had dramatic impacts on Arctic environments. In particular, the phenomenon of Arctic amplification through various feedback mechanisms has been linked to major reduction in Arctic sea-ice cover alongside major changes to the Greenland Ice Sheet (GrIS) (e.g. Dai et al., 2019; Shepherd et al., 2020). The main drivers of these changes are thought to be increased atmospheric temperatures and changes in ocean circulation bringing warmer Atlantic-sourced waters to the Arctic (van den Broeke et al., 2009; Notz and Stroeve, 2016; Polyakov et al., 2017). Recent observations

* Corresponding author.
E-mail address: J.M.Lloyd@durham.ac.uk (J.M. Lloyd).

https://doi.org/10.1016/j.quascirev.2023.108068

have estimated mass loss from the GrIS from 1972 to 2018 accounted for 9 mm sea level rise through a combination of surface melting and also, importantly, dynamic contributions (~66%) from marine-terminating outlet glaciers (MTOGs) (Mouginot et al., 2019). Recent studies have identified significant thinning, acceleration and retreat of many Greenland MTOGs (e.g. Rignot and Kanagaratnam, 2006; Straneo and Heimbach, 2013; Kochtitzky and Copland, 2022). Continued mass balance loss and dynamic contribution from MTOGs has implications not only for future sea-level rise, but also for ocean circulation, biogeochemical cycling and marine ecosystems (Catania et al., 2020; Straneo et al., 2019). The interaction between MTOGs and ocean circulation around Greenland, specifically the role of Atlantic Water, is thought to be one of the major drivers of recent change (Straneo and Heimbach, 2013; Cowton et al., 2018; Catania et al., 2020). However, there is still significant uncertainty over future mass balance changes to the GrIS with continuing climate change and the link between oceanic and atmospheric forcings (Catania et al., 2020; Fahrner et al., 2021). One way to reduce this uncertainty is to have a better understanding of the past interaction between the GrIS and the oceans, through natural climate archives – the palaeo-record.

Here we report on a marine sediment record retrieved from the continental shelf offshore of the Northeast Greenland Ice Stream (NEGIS). NEGIS is one of the largest ice stream systems in Greenland draining 12% of the GrIS and holds the equivalent to 1.1 m of sea level (Mouginot et al., 2015). NEGIS streams from the ice divide and separates into three marine-terminating outlets, Nioghalvfjerdsfjorden Glacier (79N Glacier), Zachariae Isstrøm (ZI) and Storstrømmen Glacier (SG) to the south (Fig. 1b). Up until the mid-2000s the ice shelves fringing NEGIS had been relatively stable, however, since then there has been evidence of ice shelf thinning and flow acceleration of both 79N Glacier and ZI (Khan et al., 2014). Indeed, over this time period the ZI ice shelf has completely disintegrated (approximately 40 km) and the grounded tidewater margin is now continuing to retreat (An et al., 2021). These changes are linked to a combination of increased air temperature, sea-ice loss and ocean warming (Khan et al., 2014; Mouginot et al., 2015; An et al., 2021). The 79N Glacier ends in an 80 km long ice shelf within Nioghalvfjerdsfjorden that is pinned on a series of islands at the mouth of the fjord which, along with a series of ice rises, indicates a threshold or sill at the mouth of the fjord (Bennike and Weidick, 2001). While there is evidence of thinning along the 80 km long ice shelf of 79N Glacier (one of the few remaining significant ice shelves fringing the GrIS) the ice shelf margin is still stable (Mouginot et al., 2015). How long the ice shelf will remain stable is, however, uncertain, particularly given that model predictions indicate ocean warming in this region will double by 2100 (Yin et al., 2011) and air temperatures are also predicted to increase significantly (Hanna et al., 2021).

Acoustic and seismic surveys of the continental shelf provide evidence for past advance of NEGIS to the shelf edge (Evans et al., 2009; Arndt et al., 2015, 2017). This advance has been assumed to date from the LGM based on the relatively fresh nature and limited sediment drape over glacial landforms on the shelf. The timing of retreat from the LGM position, however, is still poorly constrained. Recent research has provided minimum estimates on timing of retreat based on radiocarbon dates from sediment cores collected across the continental shelf ranging from 13.4 ka cal BP to 10.1 ka cal BP (Fig. 1b) (Syring et al., 2020; Dibattista et al., 2021; Hansen et al., 2022; Davies et al., 2022). Radiocarbon dates and cosmogenic surface exposure ages indicate the coast near NEGIS was ice free from *c.* 10 ka cal BP (Bennike and Bjorck, 2002; Larsen et al., 2018). The ice margin retreated behind the current position, and there is evidence that the ice shelf within Nioghalvfjerdsfjorden disintegrated by 8.5 ka cal BP (Smith et al., 2022).

The aim of this study is to provide a longer-term context on the interaction between NEGIS, climate change (specifically ocean circulation) and sea-ice cover across the inner continental shelf through the period of deglaciation, covering the Holocene up to the last few decades.

2. Regional setting

The northeast Greenland margin is characterised by a wide continental shelf (up to 300 km) dissected by two significant deep-water troughs, Westwind Trough to the north and Norske Trough to the south (Fig. 1b). The deep-water troughs form two arc shapes bounded by the shallower AWI Bank, Northwind Shoal and Belgica Bank. They converge at the embayment immediately east of the current 79N Glacier ice shelf. Norske Trough is approximately 350 km long and is significantly wider on the outer shelf (>200 km) narrowing to <50 km as the trough curves to a north-south orientation on the inner shelf. Water depths are approximately 400–500 m along the trough, bounded by shallower banks (200–250 m water depth).

The modern oceanography of the northeast Greenland margin is characterised by the relatively cold and low salinity Polar Water (PW) exiting the Arctic Ocean forming the East Greenland Current (temperature <0 °C, salinity <34.5), locally sourced meltwater from the GrIS and relatively warm and saline Atlantic Water (AW) sourced from the West Spitsbergen Current (temperature at the Spitsbergen margin >3 °C, salinity >34.9) (Fig. 1a). The East Greenland Current carries PW onto the northeast Greenland continental shelf circulating through the Westwind and Norske Troughs forming the upper 250 m of the water column (Budéus and Schneider, 1995; Hopkins, 1991). The PW is underlain by AW from two sources. In Norske Trough the AW is sourced directly from a branch of the West Spitsbergen Current, the Return Atlantic Current (RAC) bringing Return Atlantic Water (RAW, temperature ~2 °C, salinity 34–35) (Budéus and Schneider, 1995; Schaffer et al., 2017). The AW in Westwind Trough is significantly cooler than RAW found in Norske Trough and comes via a branch of AW circulating through the Arctic Ocean exiting Fram Strait called Arctic Atlantic Water (AAW, temperature 0.5–1 °C) (Schaffer et al., 2017). Recent studies have shown year-round flow of Atlantic Water through Norske Trough into the cavity below the 79N ice shelf and to the calving margin of ZI (Schaffer et al., 2020). Warming of this Atlantic Water inflow over recent decades has been linked to increased basal melting of the ice shelf potentially influencing the stability of the ice shelf (Lindeman et al., 2020). Cooler, low salinity melt-modified water is then exported from below the ice shelf at shallow depths (Lindeman et al., 2020).

The sea ice characteristics of this region are closely linked to the development of the Norske Øer Ice Barrier (NØIB) and the Northeast Water (NEW) Polynya that forms at the northern tip of the NØIB (Budéus et al., 1997). The NØIB is an area of semi-permanent fast-ice between 78 and 80ºN stretching 75–150 km from the coast that forms annually with variable size and thickness (Fig. 1b). Based on recent observations breakup of the NØIB was rare during the 20th century, occurred once during the 1950s then not again until 1997 (Wadhams, 1981; Reeh et al., 2001). However, since 1997, breakup of the NØIB has been observed in the summer most years (Hughes et al., 2011; Sneed and Hamilton, 2016). The presence of the NØIB and associated higher concentration of sea ice tends to reduce calving from the floating ice tongues of 79N Glacier and ZI due to the buttressing effect (Reeh et al., 2001). More regular breakup of the NØIB tends to increase calving and glacial runoff which, in turn, influences salinity of coastal waters. Sejr et al. (2017) have observed recent freshening of coastal waters in the northeast Greenland region most likely associated with increased ice sheet

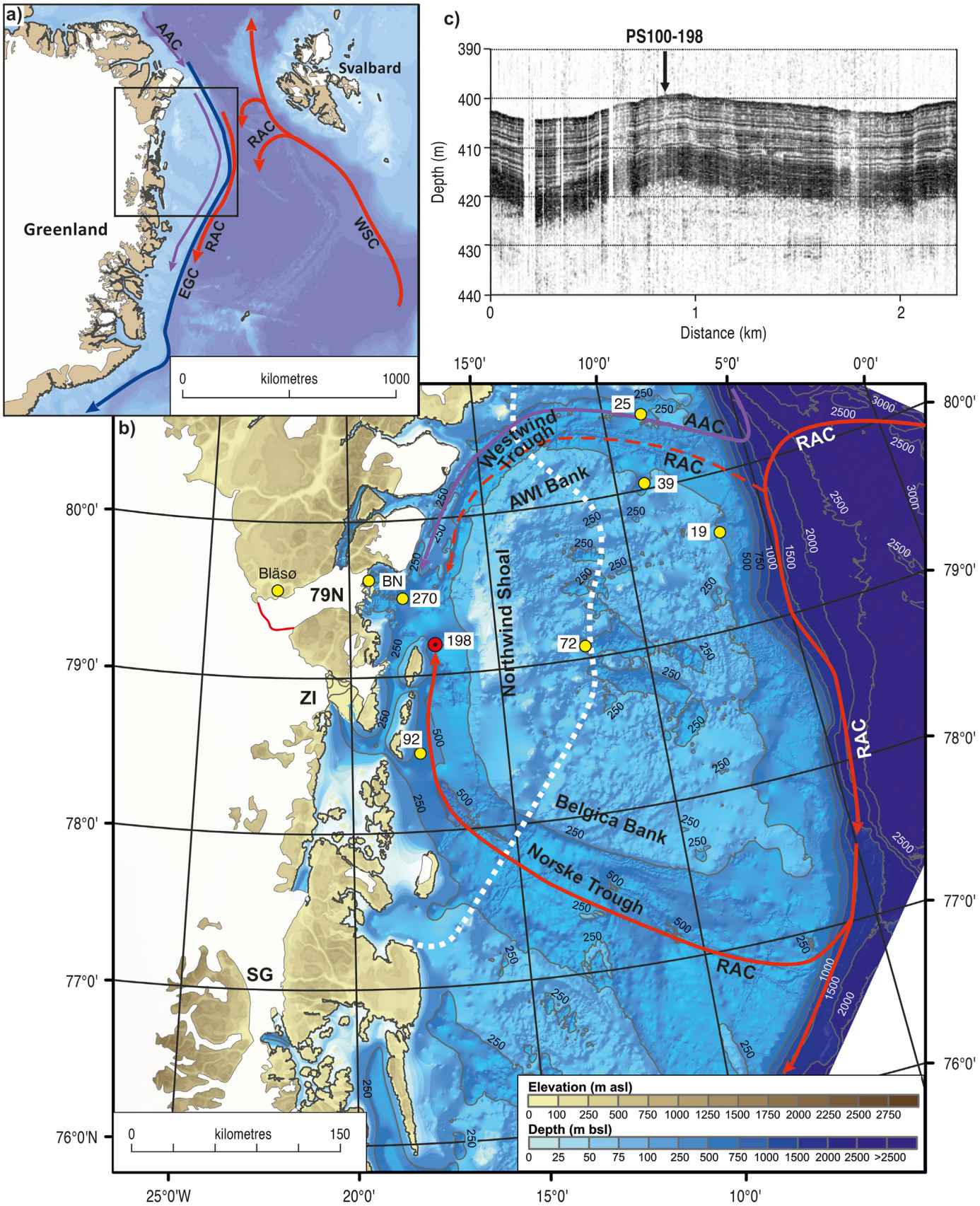

Fig. 1. (a) Overview of the study area and surface ocean circulation pattern: relatively warm currents include the Return Atlantic Current (RAC) and West Spitsbergen Current (WSC) (red), colder East Greenland Current (EGC) (blue) and the intermediate Arctic Atlantic Current (AAC) (purple). The ocean bathymetry is from GEBCO. (b) Close up of the Northeast Greenland continental shelf showing position of cores discussed in the text: 198 (red) core PS100-198 this study; 270, core PS100-270 (Syring et al., 2020); 92, core DA17-092G

melt. Such freshening of southward flowing coastal currents reduces the density of water masses that influence deepwater formation further south, potentially impacting the Atlantic meridional overturning circulation (Sejr et al., 2017). This highlights the importance of understanding the link between sea ice, ice shelf/ice stream dynamics and the ocean.

3. Material and methods

3.1. Core collection and CTD

A box core and a gravity core were collected at coring site PS100-198 during cruise PS100 of RV Polarstern in 2016 to the Northeast Greenland continental shelf. The cores were recovered from the inner section of Norske Trough, a major cross shelf trough running from the embayment immediately in front of the pinned ice shelf of 79N glacier to the continental shelf edge (79º 11.474′N, 17º 6.43′ W, water depth 398 m, Fig. 1b, Kanzow, 2017). The total core length of the gravity core PS100-198GC is 9.5 m, while the box core, PS100−198BCE, is 44 cm long and was collected to recover an undisturbed sample of the upper sediment-water interface. Once collected, the gravity core was split lengthwise, photographed and described on board before being wrapped and stored at 4 °C. The box core was photographed and described before being sub-sampled using a plastic tube and stored at 4 °C. Water temperature and salinity data were collected using a standard CTD SBE911plus system (Fig. 2) (Schaffer et al., 2020).

3.2. Physical properties

The split gravity core sections were immediately photographed, and then described recording information on sediment grain size, colour, sorting, bed contacts, clast abundance, sedimentary structures and presence of macrofossils. Post-cruise additional information was provided from core x-rays using a GEOTEK XCT scanner (box core and gravity core) and a GEOTEK Multi-Sensor Core Logger (MSCL, gravity core only) (including magnetic susceptibility and wet bulk density). Once x-rayed, the box core was extruded by pushing up through the tube and sub-sampled at 1 cm resolution.

3.3. Pb210 profile

Samples for ^{210}Pb analysis were freeze-dried and ground to a fine powder in an agate ball mill for the upper 9 cm of the box core. A known mass of homogenized sample was packed into a 40 mm PTFE tube. The sample tube was then closed with a rubber Suprasseal and the seal painted with paraffin wax to form an air tight barrier to prevent ^{222}Rn gas escape. The tubes were then left to stand for at least 21 days to allow the unsupported ^{210}Pb activities to reach equilibrium with ^{222}Rn.

The energy, FWHM and Efficiency calibrations were performed using 3 sets of certified sealed standards (Eckert & Ziegler Nuclitec GmbH) encapsulated into the same type of PTFE tubes as are used for the samples. The individual calibration standards consist of ^{210}Pb, ^{226}Ra (for ^{214}Pb) and a mixed standard of ^{241}Am, ^{137}Cs, and ^{60}Co (for ^{137}Cs). The calibration standard activities give a dead time of <7%. Sample count times were typically in excess of 450,000 s and counting errors were typically less than 10%. Monthly background counts were taken and stripped from measured spectra using the ratios of live times using EG&G GammaVision® software.

3.4. Foraminiferal analysis

A total of 80 samples were collected for foraminiferal analysis, 41 samples from the box core taken at 1 cm intervals and 39 samples from the gravity core taken at intervals ranging from 2 cm to 100 cm. Sample volume varied from 0.5 to 4 mL (cm^3) depending on foraminiferal concentration (estimated based on initial scanning of samples through the core). The variation in sample size was designed to enable approximately 300 specimens to be counted from each sample. Core samples were soaked in deionized water for several hours to help disaggregate the sediment. Foraminifera were concentrated by washing the sediment through 500 μm and 63 μm mesh sieves. The material retained on the 63 μm sieve was retained for foraminiferal analysis. Foraminifera were picked and counted from the wet residue under a binocular microscope immediately to reduce damage to agglutinated specimens and smaller, more fragile calcareous specimens. Once counted, samples were air dried to preserve material for any further analysis.

Both agglutinated and calcareous benthic foraminifera were counted along with planktic specimens. The relative abundance of individual benthic species is presented here (excluding the planktic specimens counted). Absolute abundances of benthic and planktic specimens are presented as both concentrations (number of specimens per ml of sediment) and accumulation rates or fluxes. The foraminiferal accumulation rate (FAR as individuals cm^{-2} ky^{-1}) was calculated following Ehrmann and Thiede (1985):

$$FAR = TSAR*FN$$

Where TSAR is the total sediment accumulation rate (g cm^{-2} kyr^{-1}) and FN the number of foraminifera per gram sediment.

3.5. Dinoflagellate cysts and other palynomorph analysis

Samples for marine palynological analyses were taken from the box-core only, at a resolution of 2 cm for the upper 22 cm, and 2−4 cm for the lowermost part of the core (total of 18 samples). For each sample, 2−4 g of freeze-dried sediment were prepared at the Geological Survey of Denmark and Greenland, following a standard protocol and using the *Lycopodium* marker-grain method (Mertens and Verhoeven, 2009). One *Lycopodium*-spore tablet was added to each sample prior to acid treatment. Acid treatment included removal of carbonates with room temperature 2 M hydrochloric acid (HCl) (for 24 h) and removal of silicates with room temperature hydrofluoric acid (40% HF) for up to 48 h, followed by an additional HCl treatment (24 h). The samples were then gently ultra-sonicated (30−45 s), sieved and rinsed through an 11 μm-mesh nylon filter and pH neutralized. The organic residue was collected and mounted on a microscope slide with glycerol gelatin using a heating plate. Slides were analyzed with an upright light microscope (Olympus BX51/BX60) using Differential Interference Contrast (DIC) optics at 400x or 1000× magnification. Our goal was to count a minimum of 300 cysts per sample, but this was not possible, as the core was nearly barren below 22 cm depth (only 0−7 cysts were found per sample in this interval). Besides organic-walled dinoflagellate cysts, other palynomorphs were also counted including cysts of the freshwater ciliate genus *Halodinium*. Data presented

(Davies et al., 2022); 72, core DA17-72G (Pados-Dibattista et al., 2022); 25, core PS93-025 (Zehnich et al., 2020); 39, core DA17-039G (Hansen et al., 2022); 19, DA17-019G (Rasmussen et al., 2022). White dashed line marks approximate position of the Norske Øer Ice Barrier (NØIB). Position of the three separate glaciers, Nioghalvfjerdsfjorden Glacier (79N Glacier), Zachariae Isstrøm (ZI) and Storstrømmen Glacier (SG) forming NEGIS indicated in black. Red line indicates approximate grounding line of 79N Glacier. BN − Block Nunatakker. Colour shading used to illustrate bathymetry and topography with key bathymetric features labelled. Ocean bathymetry data from Arndt et al. (2015, 2017); (c) Sub-bottom profiler data across site of core PS100-198 collected using a hull-mounted Parasound DS III-P70 system.

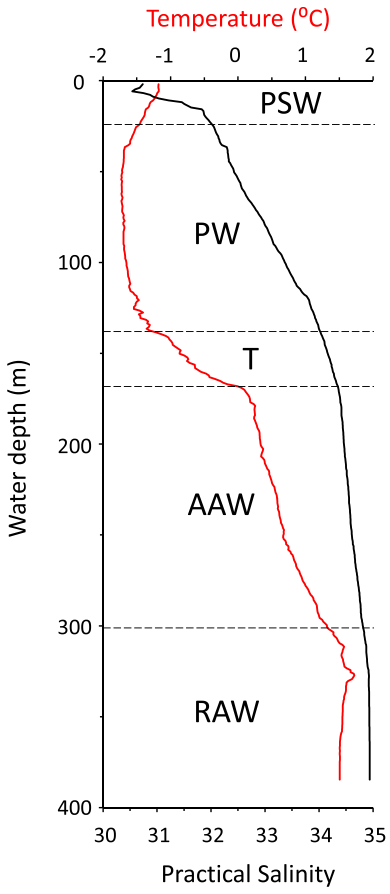

Fig. 2. CTD profile from core site PS100-198. PSW: Polar Surface Water; PW: Polar Water; T: Transition; AAW: Arctic Atlantic Water; RAW: Return Atlantic Water.

here include relative abundances of the dinocyst taxa, concentrations of *Halodinium* spp. and total dinocyst concentrations as calculated by the marker-grain method.

3.6. Diatom analysis

Samples for diatom analysis were taken from the box core only, at 2 cm resolution. Diatom slides for identification and enumeration were prepared using standard palaeoecological methods (Battarbee, 1986) at the Marine Biology Laboratory, University of Helsinki. The sediment samples were treated with 30% hydrogen peroxide for 4 h to remove organic material and with 10% hydrochloric acid to remove carbonates, and subsequently rinsed 4 times with deionized water. After the last rinse, a known concentration of microspheres was added into each sample for calculating diatom concentrations. A few drops of the cleaned sample were left to dry on cover slips and mounted onto permanent glass slides with Naphrax™. Diatom taxa were identified with a Zeiss Axio Imager.A2 research microscope, Plan-Apochromat oil immersion objective, phase contrast optics and a total magnification of × 1000. As diatom concentrations were very low, a maximum of 20 transects were counted for each slide.

3.7. Carbon analysis

The concentration of Total Carbon (TC), Total Organic Carbon (TOC) and Total Inorganic Carbon (TIC) was measured from 41 samples taken at 1 cm intervals from the box core only, using an Analytik Jena Multi Elemental Analyser 4000. For each sample sediment was freeze-dried and ball milled and weighed into ceramic boats (20–30 mg for TC, 40–50 mg for TIC). Samples for TC were combusted at a high temperature (1000–1500 °C) in the presence of oxygen. Samples for TIC were first treated with 40% orthophosphoric acid to remove the organic carbon component before combustion at high temperature (1000–1500 °C) in the presence of oxygen. In both cases the gas generated from the burning of the sample is detected by a NDIR (Non-Dispersive Infrared) detector. The instrument measures TC and TIC, then calculates TOC of the sample from the difference between TC and TIC values.

3.8. Foraminiferal stable isotope analysis

Oxygen (expressed as $\delta^{18}O$) and carbon (as $\delta^{13}C$) isotopic analyses were carried out separately on benthic and planktic foraminifera from both box core and gravity core. Approximately 20 specimens of the benthic species, *Cassidulina neoteretis*, and the planktic species *Neogloboquadrina pachyderma* were picked and measured where possible. Analyses were carried out using an IsoPrime mass spectrometer with a Multicarb preparation system at the Stable Isotope Facility in the British Geological Survey. Stable isotope results were calibrated to the VPDB scale of international standards with an analytical precision for both isotopes of > ± 0.05‰.

3.9. Sea ice biomarker analysis

A total of 20 samples were taken from the box core only (every 2 cm) and processed for HBI analysis (IP_{25} and HBI III) following the protocol described by Belt et al. (2019). An internal standard (9-octylheptadecene) was added to ~0.5 g of the freeze-dried and homogenized sediment samples before analytical treatment. Total lipids were ultrasonically extracted (3 times) using a mixture of dichloromethane (DCM: CH2Cl2) and methanol (MeOH) (2:1, v/v). Extracts were pooled together, and the solvent was removed by evaporation under a slow stream of nitrogen. The total extract was subsequently suspended in hexane and purified through open column chromatography (SiO_2). HBIs were eluted using hexane (8 mL). Procedural blanks and standard sediments were analyzed every 15 samples. Hydrocarbon fractions were analyzed using an Agilent 7890 gas chromatograph (GC) fitted with 50m fused silica Agilent J&C GC columns (0.25 mm internal diameter and 0.25 μm phase thickness) and coupled to an Agilent 5975C Series mass selective detector. Oven temperatures were programmed as follows: 40–300 °C at 10 °C min−1, followed by an isothermal interval at300 °C for 10min. The data were collected using ChemStation and analyzed using MassHunter quantification software. IP_{25} was identified on the basis of retention time and comparison of mass spectra with authenticated standards. Abundances were obtained by comparison of individual GC-mass spectrometry responses against those of the internal standard and concentrations are reported in ng g^{-1}. Response factors of the internal standard vs. IP_{25}were determined prior and after each analytical sequence (every 15 samples). The extraction and analytical error on the measurements, determined from measurements of standard sediments is ±8%.

4. Results

4.1. CTD and water masses

The water column at the core site is characterised by 4 main water masses. Between approximately 25 m and 140 m depth in the water column is the main PW layer with temperatures ranging

from −1.0 to −1.7 °C and salinity <34 (Fig. 2). Above this, the ca 25 m surface layer is composed of Polar Surface Water (PSW) that is slightly warmer due to summer insolation and has a lower salinity due to seasonal melting of sea ice and the GrIS. Below the PW is a transitional layer of increasing temperature with depth down to 170 m (from −1.7 to 0.1 °C) formed through mixing of PW with AW below. Between 170 m and 300 m the AW has a temperature 0.1 to 1.2 °C and salinity ranging from 34.4 to 34.8. This water mass has similar characteristics to the AW present in Westwind Trough (Schaffer et al., 2017) and is most likely the Arctic Atlantic Water from the AAC circulating through Westwind into Norske Trough. The deepest water mass below 300 m is the warmer AW from the RAC, temperature >1.2 °C and salinity >34.8 (Schaffer et al., 2017).

4.2. Age model and sedimentation rates

The core chronology is based on 10 accelerator mass spectrometry (AMS) ^{14}C ages (Figs. 3 and 4, Table 1) measured on mixed species of benthic foraminifera (excluding miliolids) and the ^{210}Pb profile from the box core. Four of the dates are from the box core and 6 dates are from the gravity core. AMS ^{14}C dating was carried out at the UK NERC AMS radiocarbon facility and at the Alfred Wegener Institute, Bremerhaven, using the Mini Carbon Dating System (MICADAS). Radiocarbon ages were converted to calibrated calendar years before present within the Bayesian accumulation age-depth modelling program, *Bacon 2.2* (Blaauw and Christen, 2011) using the MARINE20 calibration curve with the standard reservoir age correction of 550 years (Heaton et al., 2020; Stuiver et al., 2021). The MARINE20 calibration curve uses an increased marine reservoir correction of 550 years in comparison to MARINE13, hence a ΔR of 0 ± 0 years is used here (previously 150 ± 0 years using MARINE13) following Larsen et al. (2018).

Due to the gravity coring process the surface sediments likely were not recovered in the gravity core. The box core should have recovered the undisturbed sediment water interface. For this reason, we use the box core for the upper part of the record, then the gravity core for the longer record. We use the foraminiferal record to splice the box core and gravity core together, the base of the box core (40 cm) equates to approximately 45 cm in the gravity core (for details see Supp Info and Fig. S1). We use the full length of the box core (40 cm), then start using samples from the gravity core at the splice between the two cores from 45 cm onwards in the gravity core. A combination of the AMS ^{14}C ages from the box core and gravity core are used by *Bacon* in development of the age model (Fig. 5). Based on the ^{210}Pb profile from the box core (Fig. 5d) background levels are reached by 7 cm and an age of 130 cal BP is used by *Bacon* for this level as an additional control on the age model developed. The lowest radiocarbon date from PS100-198 gravity core at 802 cm constrains the age of the base of the core at 930 cm to *c.* 10,930 cal BP (range 10,580 to 11,510 cal BP).

4.3. Lithofacies

Based on the sediment description produced from the split gravity core sections and the box core along with additional information on sediment characteristics provided by the core x-rays and MSCL data (gravity core only), the combined core record for PS100-198 can be divided into three lithofacies. These are described in detail below and illustrated in Figs. 3 and 4.

From the core bottom, lithofacies 1 (LF1) between 930 and 86 cm gravity core depth (*c.* 10,930–9840 cal BP) consists of reddish-brown to mid-brown silty clay with very occasional clasts (Fig. 3). LF1 is characterised by colour-banded laminations more clearly illustrated in the core x-rays. The laminations are typically sub-centimetre in thickness, though occasionally there are thicker bands also present. This lithofacies is also characterised by highly fluctuating magnetic susceptibility values that gradually increase through the unit. Wet bulk density (WBD) is relatively high, decreasing gradually through this unit until a more abrupt drop at 240 cm (Fig. 4).

Lithofacies 2 (LF2) from 86 to 50 cm gravity core depth (*c.* 9840–9130 cal BP) also consists of reddish-to mid-brown silty clay with occasional clasts. The gradual transition from LF1 to LF2 is characterised by a shift to more diffuse/disturbed laminations, with some evidence of bioturbation seen in the x-rays (Fig. 3). Magnetic susceptibility reaches a peak with more stable values through this

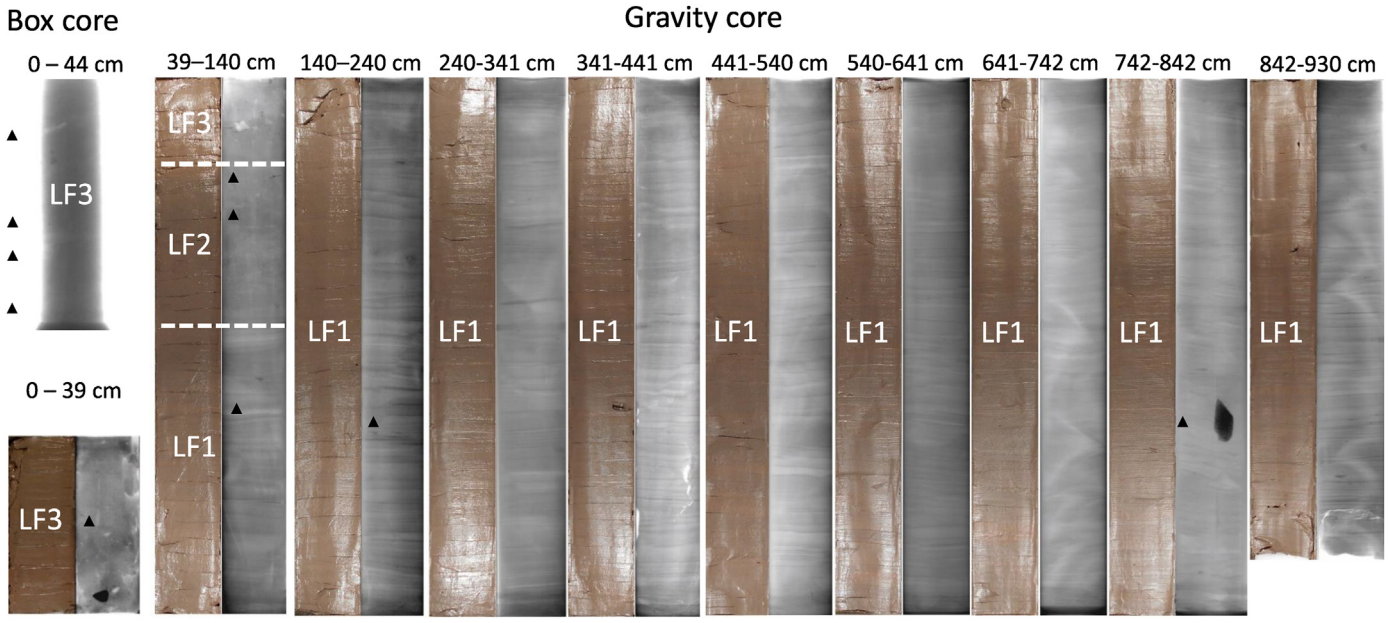

Fig. 3. X-rays and photographs of gravity core PS100-198 and x-ray of PS100-198 box core. Depth of core sections indicated. Position of radiocarbon dates shown by black triangles, position of lithofacies indicated by dashed lines.

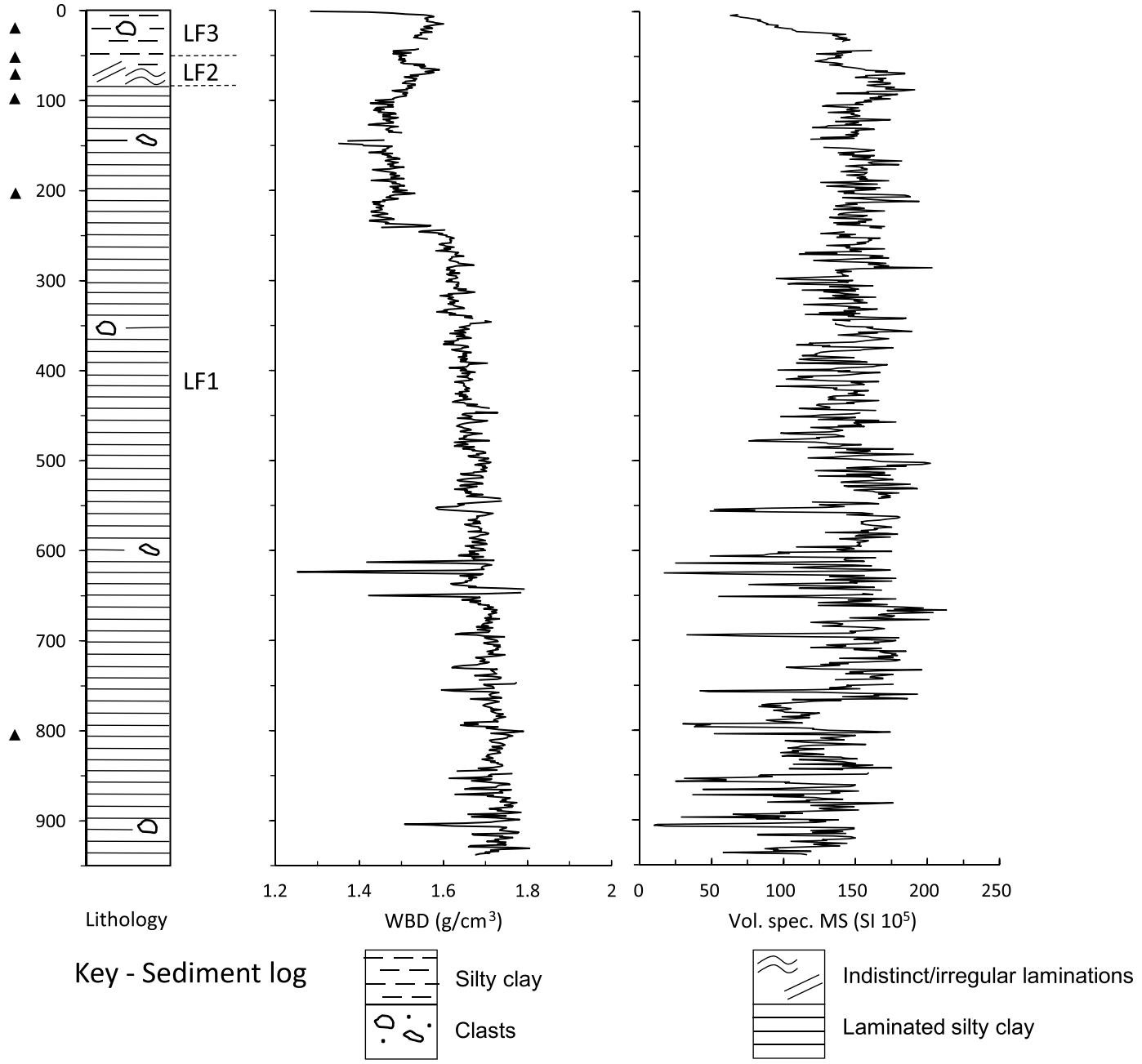

Fig. 4. Core log and physical properties (WBC: Wet Bulk Density, MS: Magnetic Susceptibility) from gravity core plotted against depth. Position of radiocarbon dates shown by black triangles and boundaries between lithofacies indicated.

unit with a slight increase in WBD values from the top of LF1 (Fig. 4).

Lithofacies 3 (LF3) from 50 to 0 cm gravity core depth and the whole of the box core (*c.* 9130 cal BP – modern) is a massive reddish-to mid-brown silty clay with a slight increase in clast abundance in comparison to LF1 and LF2 (Fig. 3). There is no evidence of laminations seen in the core x-rays and there is a decrease in MS, though still relatively stable values and WBD increases slightly in comparison to LF2 (Fig. 4).

Sedimentation rates calculated based on the age model vary significantly through the core (Fig. 5b and c) with very high rates of 780 cm kyr^{-1} within LF1 from the base of the core up to 86 cm (*c.* 9840 cal BP). At this point over the transition to LF2 there is an abrupt decrease in rates to approximately 80 cm kyr^{-1}. Sedimentation rates then gradually decrease through LF2 into LF3 to approximately 10 cm ky^{-1} by 27 cm (*c.* 8180 cal BP), then to below 4 cm ky^{-1} from 26 to 7 cm (*c.* 7925 to 130 cal BP) before increasing slightly to approximately 50 cm ky^{-1} up to present day.

4.4. Benthic foraminiferal data

The foraminiferal fauna is dominated by benthic taxa (48 benthic species, see Supp. Info. Table S1 for full species list), though planktic specimens are also common throughout the core (mainly *Neogloboquadrina pachyderma*). There is a diverse benthic foraminiferal fauna through the core dominated by calcareous species (36 calcareous species) but with one section where agglutinated species become abundant (12 agglutinated species). Overall, the core is

Table 1
AMS radiocarbon dates for box core and gravity core PS100-198. Dates are calibrated using CALIB with the Marine20 curve and a delta R of 150 following Larsen et al. (2018).

Lab Code	Depth (cm)	Material	^{14}C age	Error ±	Calib median	Calib min.	Calib max.
Box Core							
SUERC-79062	10–11	Mixed benthic forams	2070	38	1316	1174	1465
SUERC-76490	25–27	Mixed benthic forams	7742	37	7868	7716	8005
SUERC-79063	31–32	Mixed benthic forams	8379	40	8537	8377	8723
SUERC-76491	38–41	Mixed benthic forams	7106	37	7275	7133	7420
Gravity Core							
UCIAMS-211068	20–21	Mixed benthic forams	7985	40	8116	7967	8285
UCIAMS-211069	52–55	Mixed benthic forams	8770	45	9080	8897	9276
UCIAMS-211070	65–72	Mixed benthic forams	9275	40	9654	9501	9870
AWI-2796.1.1	98–100	Mixed benthic forams	9097	84	9455	9209	9702
AWI-2797.1.1	200–208	Mixed benthic forams	9206	120	9603	9276	9997
UCIAMS-216431	800–804	Mixed benthic forams	9840	70	10,425	10,205	10,658

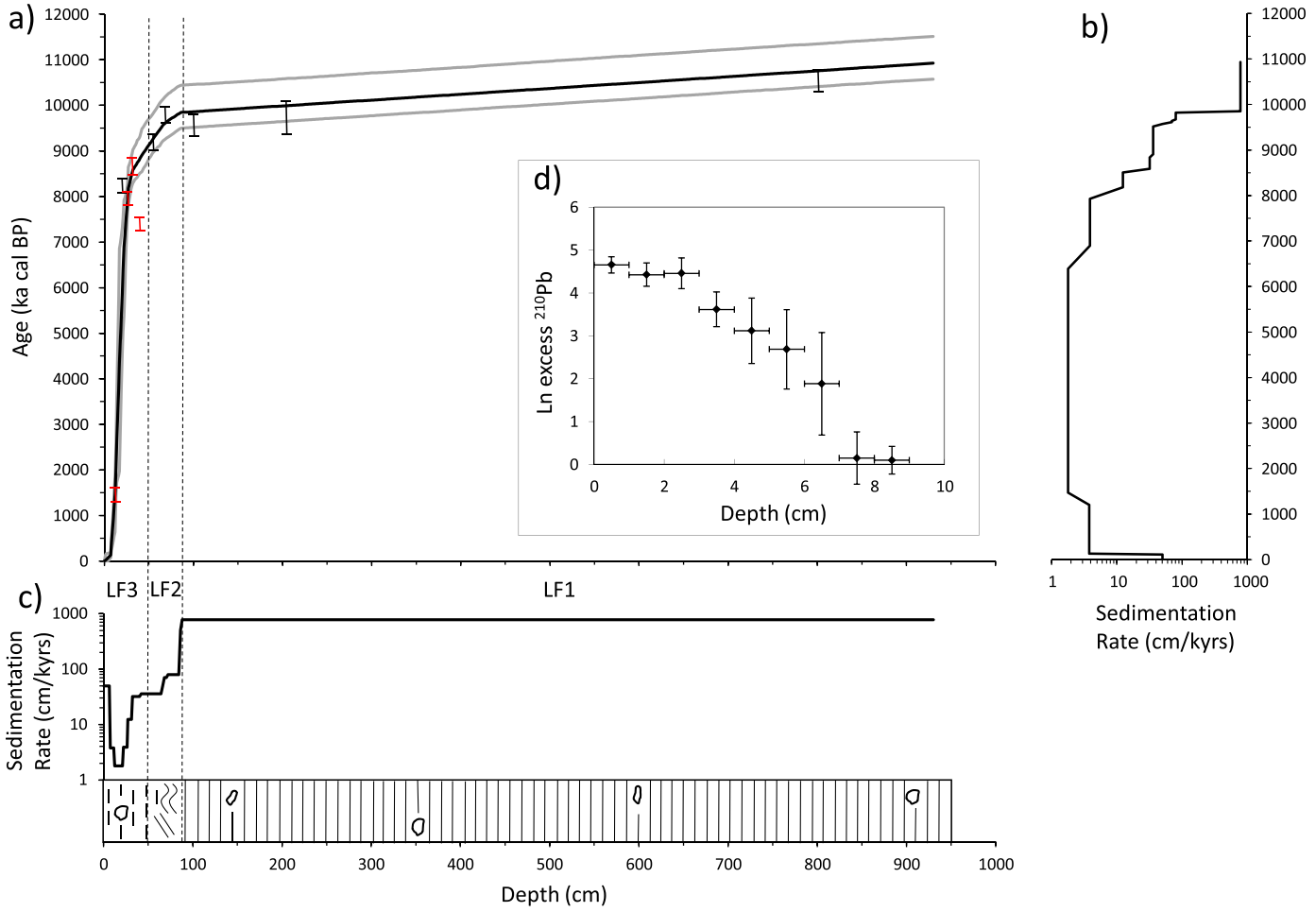

Fig. 5. a) Age model for PS100-198 spliced box core and gravity core, dates shown in red are from the box core (details of splice shown in sup info); b) Sedimentation rate plotted against age; c) Sedimentation rate plotted against depth; d) ^{210}Pb profile for PS199-198 Box Core used to provide additional age constraint for the age model shown in a). Composite lithological log and lithofacies boundaries indicated.

dominated by two key species, *Cassidulina neoteretis* and *Cassidulina reniforme* with *Nonionella iridea* and *Stainforthia feylingl* also common in some sections. The agglutinated fauna is dominated by *Spiroplectammina biformis* and *Textularia earlandi* in the lower section with *Portatrochammina karica* and *Saccamina dlifflugiformis* dominating higher up. Based on the benthic foraminiferal fauna the following 7 foraminiferal assemblage zones (FAZ) can be identified (Figs. 6 and 7).

FAZ 1 (*c.* 11,000–10,000 cal BP, 932–180 cm): this assemblage zone corresponds to the laminated unit of LF1. Foraminiferal abundance through this zone is relatively low (benthic foram accumulation rate, FAR, under 10,000 indiv. cm^{-2} kyr^{-1}). Some samples in this zone also have moderately high agglutinated foraminiferal abundance (up to 20%). The assemblage is dominated by *C. reniforme* (30–60%) and *C. neoteretis* (15–80%) with both species fluctuating very widely from sample to sample (Fig. 6). Other

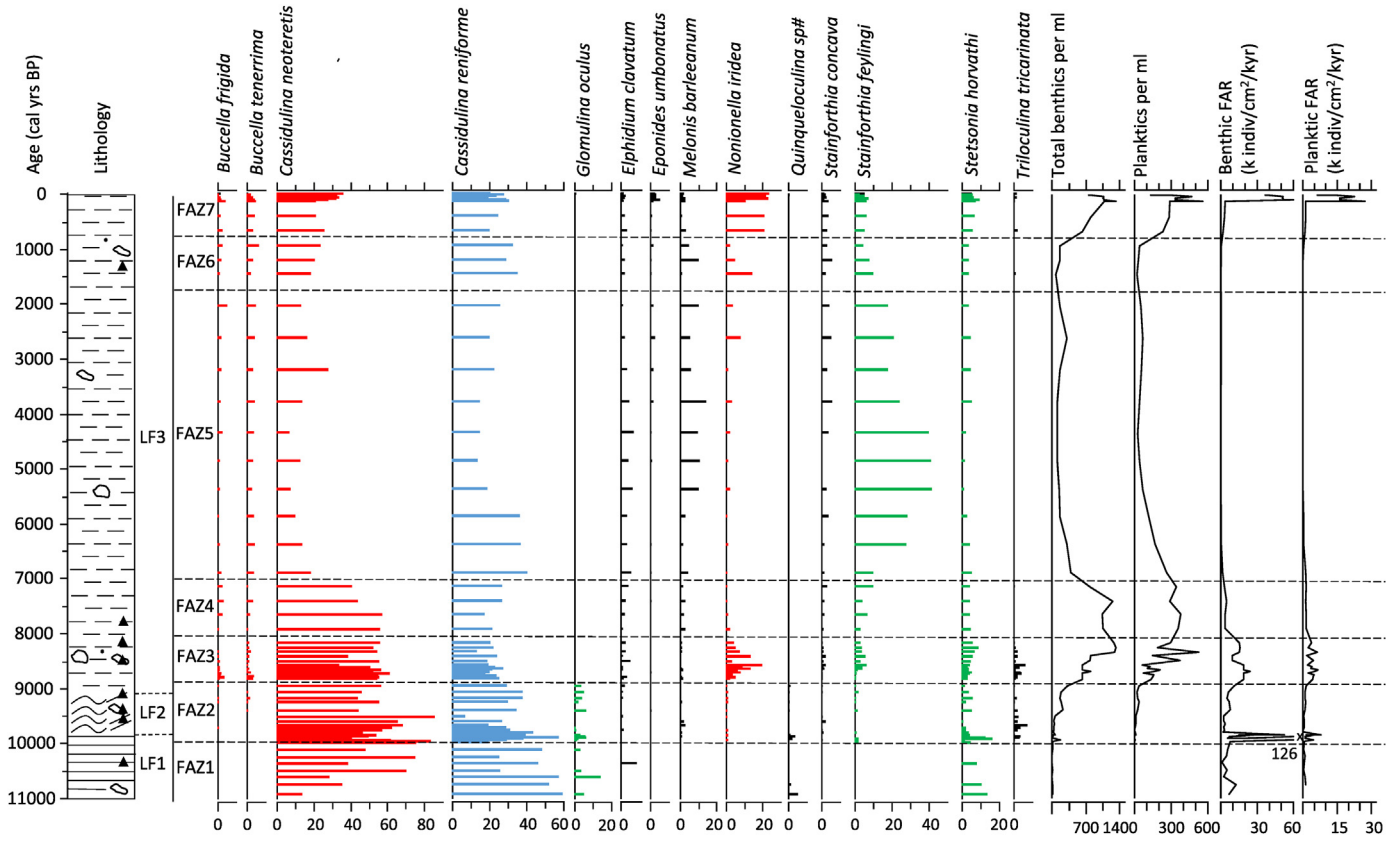

Fig. 6. PS100-198 calcareous foraminiferal assemblages from box core and gravity core spliced record, as relative abundance of calcareous foraminifera only (species >5% shown) (full data in sup info) and FAR for benthic and planktic species. Red shaded species: Atlantic Water indicators; blue shaded species: Polar Water/glaciomarine indicators; green shaded species: Polar Water/low oxygen/sea-ice indicators. Lithology and radiocarbon dates indicated, see Fig. 4 for lithology legend.

common species include *Stetsonia horvathi* and *Glomulina oculus*. The agglutinated species *Spiroplectamina biformis* and *Textularia earlandi* are also common (Fig. 7).

FAZ2 (*c.* 10,000–8900 cal BP, 180–44 cm): this assemblage zone incorporates the transition from LF1 to LF2 and into LF3 and is characterised by a peak in foraminiferal abundance at the start of the zone (up to 126,000 indiv. cm^{-2} kyr^{-1}) followed by variable, but moderate abundance. The fauna is again dominated by *C. neoteretis* and *C. reniforme* with significant fluctuations in both species, but with *C. neoteretis* slightly more dominant in comparison to FAZ1 (Fig. 6). *S. horvathi* and *G. oculus* are both common and there is a slight increase in faunal diversity. There are very few agglutinated specimens recovered in this zone (<5%).

FAZ3 (*c.* 8900–8000 cal BP, 44–27 cm): this zone is characterised by relatively high and stable benthic foraminiferal abundance (10,000–20,000 indiv. cm^{-2} kyr^{-1}) and also by an increase in planktic foraminiferal abundance (~5000 indiv. cm^{-2} kyr^{-1}). The fauna is dominated by *C. neoteretis* (30–60%) with *C. reniforme* still very common (20%) and *S. horvathi* also common (10–20%). There is a marked increase in abundance of *Nonionella iridea* through this zone, peaking at 20% mid-zone, and also an increase in abundance of several other species, *Buccella frigida*, *Buccella tenerrima* and *Stainforthia feylingi* (Fig. 6).

FAZ4 (*c.* 8000–7000 cal BP, 27–23 cm): this zone sees a drop in foraminiferal abundance, but still moderate abundances of both benthic and planktic specimens (approximately 4000 and 1200 indiv. cm^{-2} kyr^{-1} respectively). The fauna is still dominated by *C. neoteretis*, though the abundance of *C. reniforme* increases slightly towards the end of the zone and *N. iridea* reduces significantly disappearing mid-zone. There is also a slight increase in abundance of *S. feylingi* and an increasing abundance of agglutinated specimens through this zone (up to 10%).

FAZ5 (*c.* 7000–1750 cal BP, 23–13 cm): this zone covers a wide time period and is characterised by the lowest foraminiferal abundances through the core (approx. 200 indiv. cm^{-2} kyr^{-1}) and the peak in proportion of agglutinated specimens to the fauna, accounting for 30–60% of benthic foraminifera present. This zone is marked by a decrease in abundance of *C. neoteretis* (10–30%) as *C. reniforme* and *S. feylingi* co-dominate (10–40%). *Melonis barleeanus* (approx. 10%), *Elphidium excavatum* (5–10%) and *S. horvathi* (5–10%) are also common through this zone. The abundance of *N. iridea* starts off very low but increases to 5–10% by the end of the zone.

FAZ6 (*c.* 1750–800 cal BP, 13–10 cm): FAZ6 is a transitional zone with initially very low foraminiferal abundance (similar to FAZ5) but increasing at the top of the zone, with the agglutinated fauna less abundant, but still common. The fauna is dominated by a *C. reniforme* (30–40%) with *C. neoteretis* increasing through the zone (average of 20%) and *S. feylingi* decreasing through the zone (<10%). The abundance of *N. iridea* increases (5–15%) and *M. barleeanus* is also common.

FAZ7 (*c.* 800 – present, 10–0 cm): FAZ7 is characterised by increasing benthic foraminiferal abundance, initially 2000–4000 indiv. cm^{-2} kyr^{-1}, but then jumping to 35,000–65,000 indiv. cm^{-2} kyr^{-1} from *c.* 120 cal BP to present. The abundance of planktic specimens follows the same trend. This zone is co-dominated by *C. neoteretis* (20–35%), *C. reniforme* (20–30%) and *N. iridea* (20%). *S. feylingi*, *S. horvathi* and *B. tenerrima* are all common (5–10%). The upper part of FAZ7 could be considered a sub-zone (from *c.* 120 cal BP onwards) where *C. neoteretis* is the most abundance species

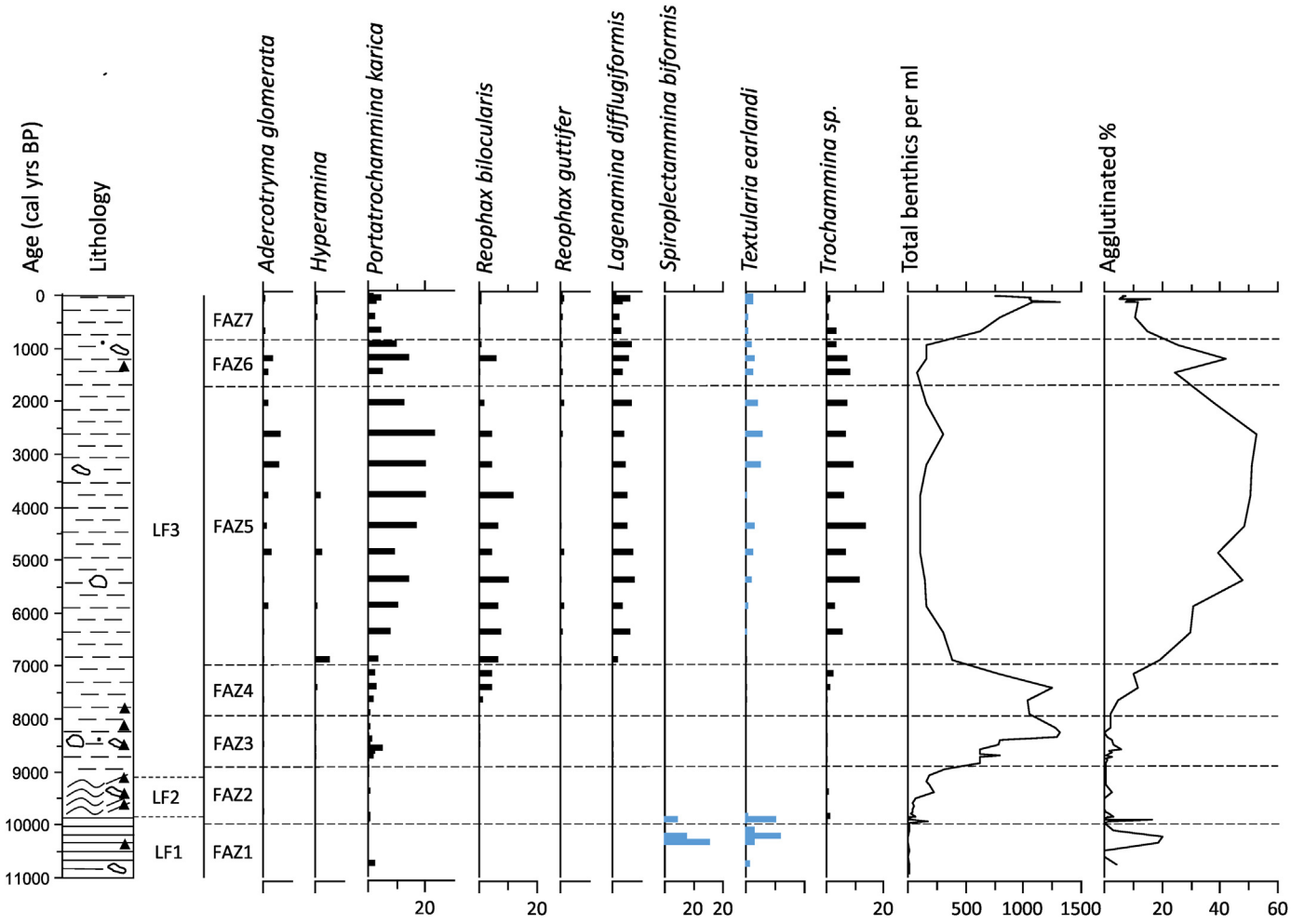

Fig. 7. PS100-198 agglutinated foraminiferal assemblage from box core and gravity core spliced record (species >2% of total foraminiferal count included) (full data in sup info). Blue shaded species: Polar Water/low salinity/meltwater indicators. Lithology and radiocarbon dates indicated, see Fig. 4 for lithology legend.

(35%) and the foraminiferal abundance jumps to >35,000 indiv. cm^{-2} kyr^{-1}. The proportion of agglutinated taxa continues to decrease to 10% or below.

4.5. Dinoglagellate cysts and other palynomorphs

Dinoflagellate cysts were investigated from the box core only, covering the period from *c.* 8900 cal yrs BP to present (Fig. 8) (see Supp. Info. Table S2 for species list). Dinocyst concentration was generally very low, particularly before *c.* 1200 cal yrs BP. The dinocyst data can be split into 3 dinocyst assemblage zones (DAZs).

DAZ1 (8900–8200 cal BP, 44–27 cm): This zone has a very low concentration of dinocysts, below 50 individuals g^{-1} dry sed, and some samples were barren. Actual counts of dinocysts are very low in this section (<10 individuals), hence relative abundances of species are rather unreliable, however, the assemblage tends to be dominated by heterotrophs such as *Brigantedinium* species (mainly *B. simplex*) and Protoperidiniacean cysts, with a few single occurrences of autotrophic taxa.

DAZ2 (8200–1200 cal BP, 27–12 cm): This zone is characterised by a slight increase in concentration (20–80 individuals g^{-1} dry sed). Actual counts are still low (5–45 individuals), however, there is a clear change in assemblage with the autotrophs *Nematosphaeropsis labyrinthus* and *Operculadinium centrocarpum* s.l. becoming dominant.

DAZ3 (1200 cal BP – present, 12–0 cm): This zone is characterised by a significant increase in concentration (90–730 individuals g^{-1} dry sed) with actual counts between 25 and 130 individuals. The assemblage is dominated by the heterotrophic species *Islandinium minutum subs. minutum* (45–50%) and *Brigantedinium* species (mostly *B. simplex*) also common (10–25%). The Arctic species *Islandinium? cezare* (1–8%) and "*Polykrikos quadratus*" (2–4%) appear in this zone for the first time. The freshwater ciliate *Halodinium* spp. reaches the highest concentrations in this interval.

4.6. Diatoms

Diatoms were also investigated through the box core. However, diatom abundance was very low with counts >10 (per 20 transects) in only the upper two samples and samples below 6 cm virtually barren. While a range of diatom species were identified (see Supp. Info. Table S3 for a full species list), the assemblage is dominated by *Chaetoceros* resting spores with the only other common species being *Fossulaphycus arcticus*.

4.7. Carbon analysis

TOC and TIC measurements were made from lithofacies 3 (Fig. 9). TOC is relatively low (below 1%) and shows an increase

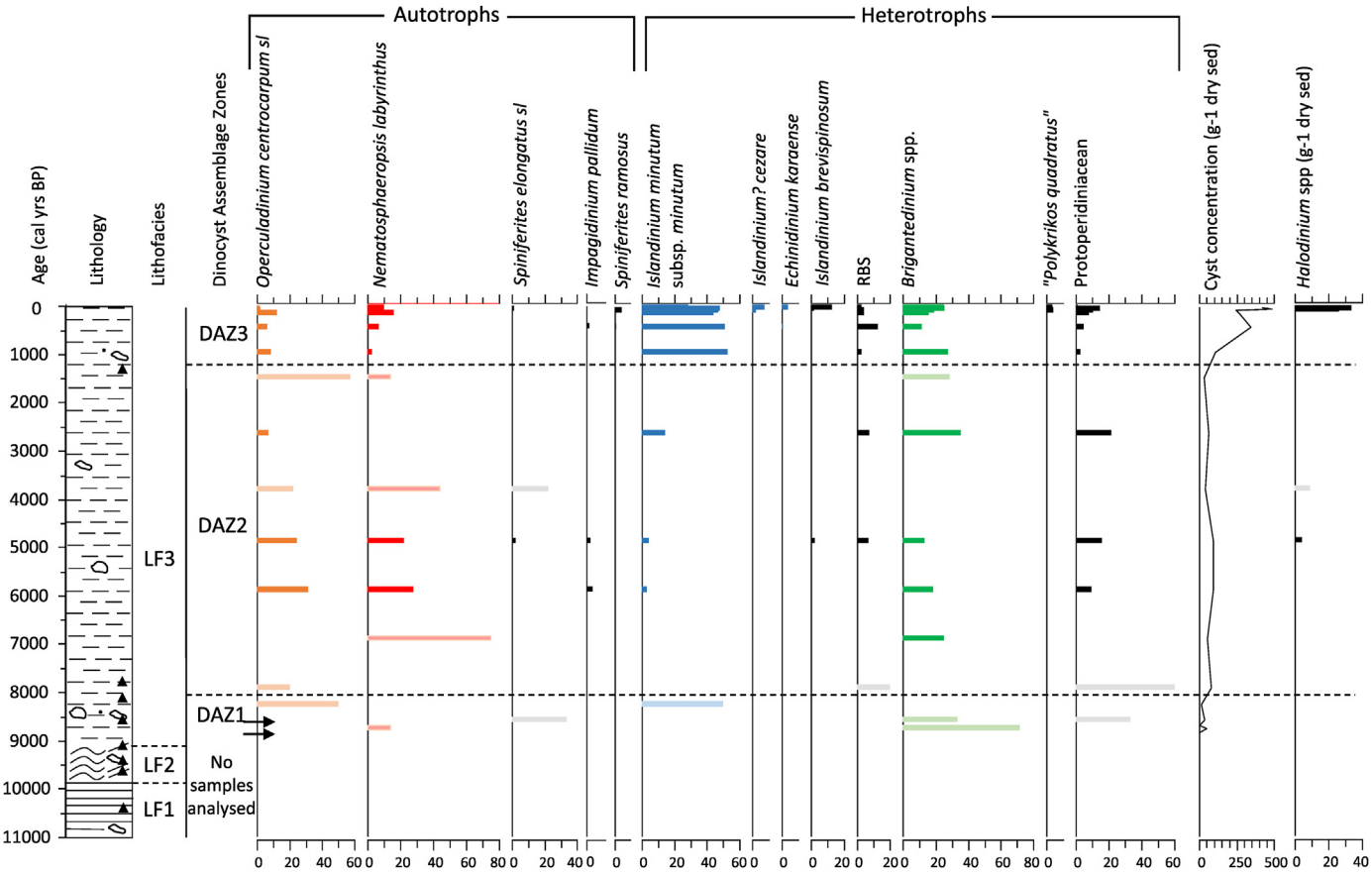

Fig. 8. PS100-198 dinoflagellate cyst assemblage from box core record (taxa present in >2 samples and >2%). Red bars: strong Atlantic Water indicator; orange bars: Atlantic Water indicator; green bars: cosmopolitan species common in seasonal sea ice; blue bars: cold water/high proportion of sea ice indicator; grey bars/paler shading indicate samples with less than 10 individuals counted. Small arrows represent position of barren samples. Lithology and radiocarbon dates indicated, see Fig. 4 for lithology legend.

from 0.20% at the base of the box core (41 cm) to a peak of 0.63% at the surface. TIC shows a decreasing trend from a maximum of 0.70% at the base of the core to a minimum of 0.33% at 10 cm, then a slight increase to 0.50% at the core surface.

4.8. Stable Isotopes

The benthic foraminiferal $\delta^{18}O$ profile shows relatively high, but highly variable values (+3.6 to +4.5‰) at the base of the core from *c.* 11,000–9000 cal yrs BP (Fig. 9). Between *c.* 9000 and 400 cal yrs BP values are relatively stable (+3.6 to +3.8‰) with a slight decrease over the last 100 yrs (+3.5 to +3.6‰). The benthic $\delta^{13}C$ profile shows relatively low, but highly variable values (−0.3 to +0.9‰) at the base of the core (*c.* 11,000–9400 cal yrs BP). This is followed by a gradual trend to higher values stabilising at approximately −0.3‰ from *c.* 8500–5000 cal yrs BP. There is a slight decrease in values at *c.* 3700 cal yrs BP followed by an increase to peak of −0.4‰ at *c.* 1000 cal yrs BP and a slight decrease over the last 100 yrs.

The planktic foraminiferal $\delta^{18}O$ profile shows relatively high values (+3.0 to +3.5‰) from *c.* 11,000–8800 cal yrs BP, with a brief interval of heavier values from 9700 to 9500 cal yrs BP (Fig. 9). From this point onwards values gradually decrease to +2.0‰ by *c.* 3700 cal yrs BP. Resolution is then rather low but, with the exception of one sample at *c.* 1000 cal yrs BP, values remain at approximately 2.0‰. The planktic $\delta^{13}C$ profile starts with relatively low values (averaging +0.3‰) from *c.* 11,000–9500 cal yrs BP then gradually increases to +0.6 to +0.7‰ by *c.* 8300 cal yrs BP. The $\delta^{13}C$ values then remain stable until increasing to +0.8 to +0.9‰ from *c.* 400 cal yrs BP to present.

4.9. Sea ice biomarkers

The concentration of IP_{25} is generally very low through most of the samples analyzed (Fig. 9). The profile can be divided into three sections. The lower section analyzed (*c.* 8800–6900 cal yrs BP) has no IP_{25} detected in the samples. Then from *c.* 5900–400 cal yrs BP IP_{25} is present in very low concentrations <0.4 ng/g. After this point concentrations rise sharply peaking at 9 ng/g at the surface sample (recent). The biomarker HBI III (Triene) was not detected in any of the samples analyzed from this record.

5. Discussion

This study aims to investigate the interaction between NEGIS, climate change (specifically ocean circulation) and sea-ice cover through deglaciation up to the present. The changes in sediment stratigraphy summarised by the three lithofacies identified along with estimates of changes in sedimentation rate provide important information on ice margin retreat and proximity of the core site to the grounding line. The benthic foraminiferal assemblages provide additional information on interaction between ocean circulation and the dynamics of the ice margin, in particular the presence and strength of subsurface Atlantic Water on the inner continental shelf through the flow of the RAC along the Norske Trough. In addition, the range of surface water proxies presented allow us to reconstruct

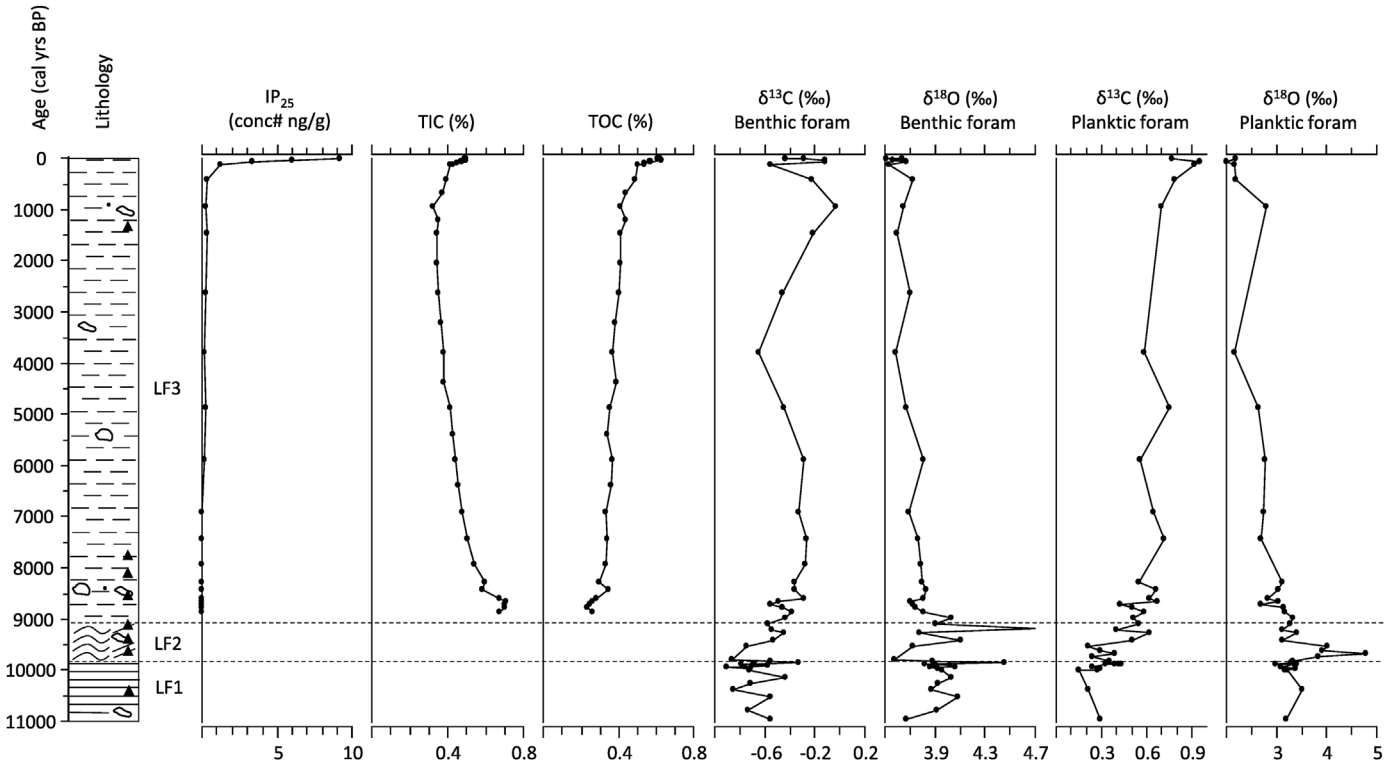

Fig. 9. PS100-198 IP_{25}, total inorganic carbon and total organic carbon concentration (from box core only), foraminiferal oxygen and carbon stable isotopes from spliced box core and gravity core. Lithology and radiocarbon dates indicated, see Fig. 4 for lithology legend.

surface conditions, in particular the relative concentration of sea-ice cover and the interaction between the ice margin (potentially an ice shelf margin) and surface water conditions. In the section below we provide an environmental interpretation drawing on this wide range of analyses.

5.1. Early holocene (10.9–10 ka cal BP) – deglaciation and a proximal glaciomarine environment

The lowest unit in PS100-198 (LF1 and FAZ1) comprises thinly laminated fine-grained sediments with a very high sedimentation rate (780 cm $kyrs^{-1}$) (Figs. 3 and 5). This most likely reflects sedimentation in a proximal glaciomarine environment with large volumes of sediment-laden meltwater production from the grounding zone (cf. Ó Cofaigh and Dowdeswell, 2001). Coarse clasts are rare throughout the record and sand content is very low indicating iceberg rafting is not an important process in sediment delivery at this site. Similar deposits are preserved in other cores from Norske Trough, DA17-NG-ST08-092G (hereafter DA17-092G) located within the main Norske Trough approximately 80 km to the south and PS100-270 located approximately 50 km to the north in the embayment in front of 79N Glacier where Westwind Trough and Norske Trough meet (Davies et al., 2022 and Syring et al., 2020 respectively, Fig. 1b). Core PS100-198 does not penetrate into a subglacial till that was recovered in PS100-270 (Syring et al., 2020). Indeed, the seismic section across the core site shows a very thick parallel laminated unit (Fig. 1c); core PS100-198 has only sampled the upper 10 m of this unit. Hence the basal age of our core, *c.* 10.9 ka cal BP (range of 10.6–11.5 ka cal BP), provides a minimum estimate of deglaciation at this core site.

Initially from *c.* 10.9 to 10.5 ka cal BP the foraminiferal fauna is dominated by *C. reniforme* (Fig. 6), a species indicative of cold Polar Waters, often associated with seasonal sea-ice cover and glaciomarine environments (Hald and Korsun, 1997; Polyak et al., 2002). Two other common species, *S. horvathi* and *G. oculus*, also indicate harsh conditions. *Stetsonia horvathi* is found in areas of extensive sea ice cover, often below an ice tongue or ice shelf, and in glaciomarine environments (Jennings et al., 2020a; Wollenburg and Mackensen, 1998), while *G. oculus* is common close to marine-terminating glaciers often associated with mobile pack ice (Jennings et al., 2020b). This suggests an initial proximal glaciomarine environment dominated by cold Polar Waters below heavy sea-ice cover or even an ice tongue/shelf environment after initial deglaciation (Figs. 10d, g and 11a, b). However, *C. neoteretis*, a typical indicator of Atlantic sourced water along many Arctic continental margins (Cage et al., 2021; Jennings et al., 2004; Jennings and Helgadottir, 1994; Knudsen et al., 2004), is also present and increases in relative abundance through this zone. This indicates the presence of RAW in this region immediately on deglaciation. The highly variable and fluctuating abundance/dominance of *C. neoteretis* and *C. reniforme* through this interval indicates a highly variable environment close to the grounding line with pulses of meltwater diluting the flux of RAW to the area. Such highly variable conditions are also supported by the relatively high, but also variable benthic $\delta^{18}O$ values (cold water with influence of isotopically light meltwater pulses, Fig. 9). Cold, variable salinity PW influence is also supported by the relatively high proportion of the agglutinated species *T. earlandi* and *S. biformis* (Jennings and Helgadottir, 1994; Korsun and Hald, 2000; Jennings et al., 2020a). This agrees with other studies from the region identifying the presence of Atlantic sourced water immediately on deglaciation from *c.* 13 ka cal BP in outer Westwind Trough to the north (core DA17-039G, Fig. 1b; Hansen et al., 2022) and mid-Norske Trough to the south (core DA17-092G, Figs. 1b and 10d; Davies et al., 2022). This correlates well with relatively cold, but warming subsurface water temperatures in the Fram Strait (Fig. 10b).

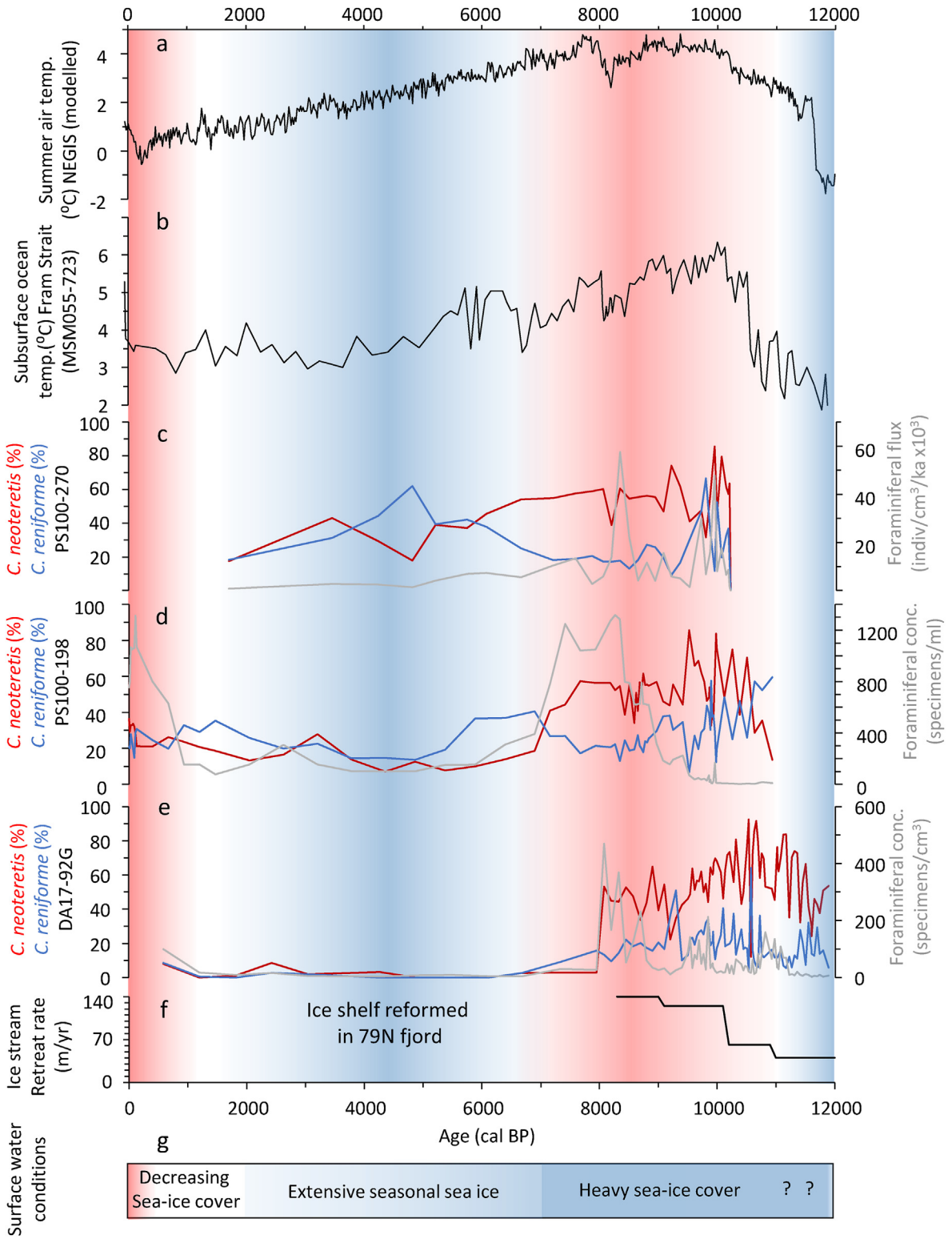

Fig. 10. a) Modelled summer air temperature in the NEGIS region (Buizert et al., 2018); b) Transfer function derived subsurface ocean temperature from Fram Strait (Werner et al., 2016); c) Summary benthic foraminiferal data from PS100-270 (Syring et al., 2020); d) Summary foraminiferal data from PS100-198 (this study); e) Summary foraminiferal data from DA17-092G (Davies et al., 2022); f) Estimated ice stream retreat rate; g) Qualitative sea-ice cover conditions based on range of proxies (this study). Panels a) to f), graded blue shading indicates relatively cold subsurface waters, weak RAC advection through Norske Trough; graded red shading indicates relatively warm subsurface waters, strong RAC advection through Norske Trough. Panel g) blue shading indicates heavy sea-ice cover, grading to seasonal sea-ice cover; graded red shading indicates decreasing seasonal sea-ice cover.

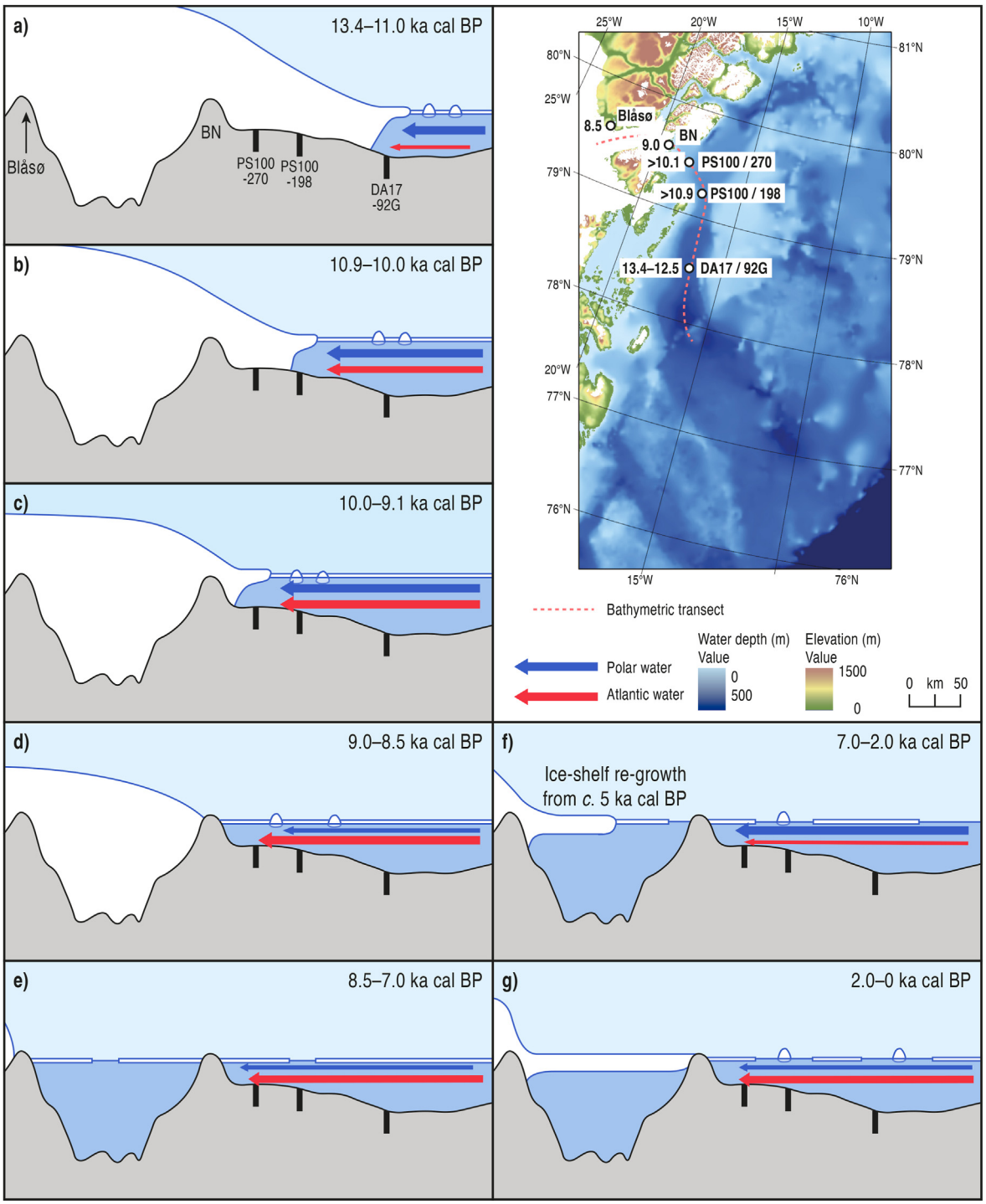

Fig. 11. Conceptual model representing the interaction between the marginal position of 79N Glacier, ocean circulation and sea ice cover. Panels a) to g) represent key time intervals discussed in the text. Ocean bathymetry data illustrated on the map and in the cross sections is from Arndt et al. (2015, 2017). Position of bathymetric cross section in panels a) to g) shown by red dashed line on map. Position of offshore sediment cores, island of Block Nunatakker (BN) and Blåsø Lake shown on map along with estimates of age of deglaciation at each location. The thickness of coloured arrows indicates stronger/weaker influence of East Greenland Current in blue and relatively warm Atlantic water in red.

5.2. Early holocene (10–9.1 cal ka BP) – retreating ice sheet

This transitional period is marked by a significant reduction in sedimentation rate to approximately 80 cm kyrs^{-1} at the start of this period reducing gradually to 36 cm kyrs^{-1} by the end (Fig. 5). This period equates to LF2, and most of FAZ2, with increasingly diffuse and disturbed sediment laminations with evidence of bioturbation towards the top of LF2. These sedimentological characteristics suggest the core site is becoming more distal to the grounding margin as the ice sheet retreats (north)westwards and is accompanied by an increase in productivity leading to bioturbation. Initially there is a peak in foraminiferal accumulation rates (both benthic and planktic) supporting increased productivity (Fig. 6). The fauna is similar to before, but with a slightly increased

dominance of *C. neoteretis* and with still variable co-dominance of *C. reniforme* (Fig. 6). The fauna indicates the persistence of variable conditions, with good evidence for heavy sea-ice cover (*S. horvathi* and *G. oculus* still common), but also for an increasing influx of subsurface Atlantic Water through a stronger RAC (Fig. 10d). The foraminiferal $\delta^{18}O$ values still show significant variation indicating fluctuating conditions (Fig. 8). There is an anti-phase relationship between planktic and benthic $\delta^{18}O$ records suggesting strong vertical stratification in the water column. Agglutinated taxa decrease significantly (Fig. 7) supporting an inference of ameliorated conditions most likely associated with the gradual retreat of the grounded ice margin as the core site records a more distal glaciomarine environment. This period coincides with the peak in Holocene modelled summer air temperatures in the NEGIS region (Buizert et al., 2018) and also the peak warmth of subsurface Atlantic Water in Fram strait (Werner et al., 2016) (Fig. 10a and b). Our interpretation of relatively warm subsurface Atlantic Water (Fig. 11c) also matches foraminiferal-based reconstructions from nearby cores in Norske Trough, DA17-092G and PS100-270 (Fig. 10c and e). Zehnich et al. (2020) also record strong advection of RAC onto the outer shelf at core PS93-025 (Fig. 1b) between from 10 to 8 ka cal BP.

5.3. Early holocene – peak sub-surface warmth and harsh surface conditions (9.0–7.0 ka cal BP)

Moving into the lower section of LF3 (FAZ3, DAZ1) there is a continued reduction in sedimentation rate (36 reducing to 12 cm $kyrs^{-1}$, then a further reduction to 4 after *c.* 8 ka cal BP) as laminations disappear and the sediment becomes a massive bioturbated silty clay with rare clasts. There is a significant increase in benthic and planktic foraminiferal abundance indicating increased productivity (equating to FAZ3, Fig. 6). However, other surface water proxies indicate very low surface productivity (DAZ1, Figs. 8 and 9) – no diatoms were found along the analyzed transects and dinocysts, while present, are in very low concentrations (with actual counts <10). The sea ice biomarker, IP_{25}, found in marine sediments underneath seasonal sea ice (Belt et al., 2007; Belt and Müller, 2013), is also absent from this interval. Interpreted together with other proxy evidence, the absence of IP_{25} suggests continued heavy sea-ice cover, potentially with low productivity through mobile heavy sea-ice cover (Fig. 10g). The presence of planktic foraminifera in this period may indicate advection across the continental shelf, or that they are living below the relatively harsh surface water conditions. The $\delta^{13}C$ signal from the planktic foraminifera shows a trend to higher values potentially indicating an increase in surface productivity below a mobile heavy sea-ice cover, or may relate to conditions further offshore if the foraminifera are advected across the shelf within the RAC flow (cf. Pados et al., 2015). The increase in concentration of benthic foraminifera indicates increased sea-floor productivity and an increase in the strength of Atlantic Water flux through the RAC at the core site. *Cassidulina neoteretis* dominates (consistently 50–60%) while *C. reniforme* reduces slightly. There is also a noticeable increase in *Nonionella iridea*, peaking at 20% at *c.* 8.5 ka cal BP during this interval before reducing to lower values < 5% after *c.* 8.0 ka cal BP (within FAZ4, Fig. 6). This is a phytodetritus feeder often associated with pulsed delivery (Gooday and Hughes, 2002), but also associated with Atlantic Water around the Greenland margin (Jennings et al., 2020a). The benthic foraminiferal data within FAZ3 indicates a peak in RAC flux and, hence water temperature, associated with an increase in productivity between *c.* 9.0 and 8.0 ka cal BP (see Fig. 11d).

This period marks the continued retreat of the grounding line recorded by reduced sedimentation rates and the development of a relatively strong (warm) RAC flow reaching mid-to inner Norske Trough. Other cores in Norske Trough also indicate a strong RAC flow at this time (DA17-092G and PS100-270, Fig. 10c and e). This period also coincides with continued (but slightly reduced) warm subsurface ocean temperatures in Fram Strait (Fig. 10b) and the outer shelf (until *c.* 8 ka cal BP; Zehnich et al., 2020) and warm air temperatures in the NEGIS region (Fig. 10a). However, conditions recorded in core DA17-NG-ST7-73G (hereafter DA17-73G) on the shallower inter-trough bank area to the north and in core DA17-NG-ST03-039G (hereafter D17-039G) from outer Westwind Trough (Fig. 1b) suggest a slightly later peak in subsurface warmth (8.2–6.2 ka cal BP, Pados-Dibattista et al., 2022 and 7.5–6.7 ka cal BP, Hansen et al., 2022 respectively). This difference in timing may be due to variations in stratification and the routing of RAC through the deeper Norske Trough. While this period marks a peak in subsurface ocean temperatures in Norske Trough, it coincides with continued harsh surface water conditions with, most likely, heavy sea-ice cover (lower section of DAZ2, Fig. 8). This suggests very strong vertical stratification with surface waters potentially still strongly influenced by the rapidly melting and retreating ice sheet (large volumes of meltwater flux). Such an anti-phase relationship between surface and subsurface conditions has also been observed in the Disko Bay region of West Greenland (Moros et al., 2016).

5.4. Mid to late holocene –neoglacial cooling (2.0–7.0 ka cal BP)

This period represents the coldest/harshest bottom water conditions illustrated by the benthic foraminifera (FAZ5, Figs. 6 and 11f) with *C. neoteretis* reaching the lowest abundances through the core (10–30%) while *C. reniforme* increases initially then decreases as *Stainforthia feylingi* (a species that tolerates unstable conditions often associated with sea-ice edge/seasonal sea ice, Knudsen and Seidenkrantz, 1994; Patterson et al., 2000) becomes (co)-dominant (20–40%). The significant increase in relative abundance of agglutinated fauna (increasing to 20–40% of the total fauna, Fig. 7) supports an interpretation of relatively harsh basal conditions (e.g. Schroder-Adams et al., 1990; Jennings et al., 2020a). The surface water proxies, in contrast, indicate a continued anti-phase relationship with a slight increase in productivity and amelioration in conditions. Dinocysts are still relatively sparse, but several samples have high relative abundances of *Operculodinium centrocarpum* and *Nematosphaeropsis labyrinthus* (DAZ2, Fig. 8), two open-water species very abundant in the North Atlantic Ocean and considered to have an affinity for relatively warmer and saltier conditions (Rochon et al., 1999; Zonneveld et al., 2013, 2013de Vernal et al., 2020). The relatively high abundances of heterotrophic *Brigantedinium* cysts in this interval is indicative of increased productivity (de Vernal et al., 2020). Although no diatoms were found through this interval very low concentrations of IP_{25} were present (<0.3 ng/g) indicating extensive sea-ice cover (Belt and Müller, 2013). The $\delta^{13}C$ signal from planktic foraminifera records relatively high values supporting an interpretation of increased productivity (Fig. 9). The relatively low $\delta^{18}O$ planktic values most likely reflects an increase in meltwater in the surface waters (cf. Pados et al., 2015). These surface water proxies indicate a transition from relatively heavy to seasonal sea-ice cover with delivery of meltwater and nutrients to the surface waters and variable influx of Atlantic Water at the surface, but still rather harsh surface conditions (Fig. 10g). The presence of some open water/sea-ice edge conditions is also supported by the presence of *Melonis barleeanum* and the increase in abundance of *S. feylingi* – the former often associated with an influx of organic matter (Corliss, 1991; Lloyd, 2006) and the later often associated with sea-ice edge conditions with corresponding increase in surface productivity (Seidenkrantz, 2013). Sedimentation rates through this interval are very low

(<2 cm kyrs^{-1}) indicating a distal grounded margin (within 79N fjord). A reduced RAC flow through Norske Trough at this time is also indicated by cores DA17-092G and PS100-270 (Fig. 10c, e) and this also coincides with a period of relatively cold bottom waters in Westwind Trough (Hansen et al., 2022) and reduced RAC advection onto the continental shelf (Zehnich et al., 2020). This period also coincides with cool subsurface ocean temperatures in Fram Strait and gradual atmospheric cooing (Fig. 10a and b).

5.5. Late holocene (2.0–0.1 ka cal BP) – seasonal sea ice

The benthic foraminiferal assemblage indicates an increase in RAC flow across the inner continental shelf (slight increase in abundance of *C. neoteretis* as *N. iridea* increases to 20% and *S. feylingi* reduces and the proportion of agglutinated taxa also reduces, FAZ6 through FAZ7, Figs. 6 and 7) (see Fig. 11g). The surface water proxies indicate an increasingly seasonal sea ice regime (with a more prolonged open water season, Fig. 10g), as evidenced by the increase in *Islandinium minutum* subs. *minutum* and the appearance of *Islandinium? cezare* (equating to DAZ3, Fig. 8) (Head et al., 2001, 2001de Vernal et al., 2020). The concentration of IP_{25} increases slightly (more open water potentially) and the planktic foraminiferal $\delta^{13}C$ values continue to increase slightly indicating increasing surface water productivity (Fig. 9). Increased surface water productivity is also supported by the increase in total dinocyst concentrations. Surface air temperatures continue to cool during this period, while subsurface ocean temperatures remain relatively low, but with a slight increase (Fig. 10a and b).

5.6. Historical period (0.1 ka cal BP – present) – decreasing sea-ice cover

The lithostratigraphy recording in the last *c.* 100 years remains unchanged, massive silty clay, however, our proxies indicate significant changes in both surface and bottom water conditions. While sedimentation rates increase slightly over this period, all proxies indicate an increase in productivity and/or preservation of biogenic material. The concentration of TOC, though still rather low, reaches a peak of 0.6% (Fig. 9). Foraminiferal accumulation rates for both planktics and benthics also reach relatively high values (Fig. 6). The surface water proxies indicate a significant increase in surface productivity, planktic $\delta^{13}C$ values reach the highest levels through the core (Fig. 9), dinocyst concentrations also reach peak values (through DAZ3, Fig. 8) and diatoms, though still sparse, reach the highest levels through the core at the surface. The benthic foraminiferal fauna indicate significant warming of subsurface water reaching similar conditions to the early Holocene peak (*C. neoteretis* increasing to 30–40%, *N. iridea* above 20%, uppermost section of FAZ7, Fig. 6). The dinocyst assemblages indicate continued seasonal sea-ice formation and melt; dominated by the cold-water and sea-ice associated species *I. minutum* and other species commonly associated with seasonal sea ice (e.g. *I? cezare*). The IP_{25} concentration shows a significant increase through this period rising to a peak of 9 ng/g at the surface. Taken together, the increase in surface productivity and increasing concentration of IP_{25} suggests a decrease in sea ice cover over the last 100 years (Fig. 10g). Over the last 100 years there appears to have been a shift with surface and subsurface proxies now in-phase and indicating relatively warm conditions.

There are very few records with which to compare our reconstruction of the last 100 years. We know from recent CTD casts that there has been an increase in the temperature of Atlantic Water reaching the cavity below the ice shelf of 79N Glacier from at least 1998 onwards (Mayer et al., 2018; Lindeman et al., 2020). While the velocity and ice-front position of 79N Glacier has been relatively stable over this period, Zachariae Isstrøm has accelerated and the ice shelf has disintegrated since 2002–2003. The resolution from our record is not high enough to identify this trend with confidence. However, our surface proxies indicate conditions are at their warmest in historical times (unprecedented over the past *c.* 9 ka cal BP) and subsurface conditions are as warm as during the early Holocene peak (immediately prior to the break-up of the ice shelf within 79N fjord before *c.* 7.7 ka cal BP, Bennike and Weidick; 2001) (see Fig. 11). This points to the susceptibility of the current ice shelf within 79N fjord to break up if conditions persist.

5.7. Timing of deglaciation and rate of ice stream retreat

The timing of glacial retreat across the northeast Greenland shelf from the Last Glacial Maximum (LGM) is still rather poorly constrained. While the ice sheet is thought to have reached the shelf edge through Westwind and Norske Troughs (presence of mega-scale glacial lineations), there is no direct dating control on this and the timing of retreat from this maximum position is unclear (Arndt et al., 2015, 2017; Larsen et al., 2018). However, Rasmussen et al. (2022) suggest the shelf edge immediately south of Westwind Trough (core 19, Fig. 1b) was not glaciated during the LGM. Indeed, the benthic foraminiferal assemblage from this core indicates the core site was influenced by Atlantic sourced water through the LGM. One of the earliest dates on deglaciation has been reported by Hansen et al. (2022) from a core in outer Westwind Trough, DA17NG-ST03-039G. The basal age from this core of *c.* 13.3 ka cal BP is a minimum age on deglaciation for the outer Westwind Trough. The signature of ice retreat across the shelf in both Norske Trough and Westwind Trough is recorded in grounding zone wedges and also moraines (Evans et al., 2009; Winkelmann et al., 2010; Arndt et al., 2017). Based on core DA17-092G (Fig. 1b), the timing of deglaciation through the southern section of inner Norske Trough has been estimated to 13.4–12.5 ka cal BP (Davies et al., 2022) (see Fig. 11 for estimated retreat of NEGIS through Norsk Trough). The basal age reported here (*c.* 10.9 ka cal BP) acts as a limiting age for deglaciation through inner Norske Trough. Syring et al. (2020) record the retreat of the ice margin into the inner shelf embayment in front of the current 79N ice shelf by *c.* 10.1 ka cal BP. Radiocarbon dates from the outer coast near 79N Glacier show the coast was ice free by 9.7 ka cal BP (Bennike and Bjorck, 2002). Cosmogenic surface exposure ages (^{10}Be) from Bloch Nunatakker, an island at the mouth of 79N fjord and currently acting as a pinning point for the 79N ice shelf, indicate the ice shelf retreating inland of the current position between 8.6 and 9.2 ka BP (an average age of 9.0 ka BP based on three dates, Larsen et al., 2018).

Taking the mid-point of the estimated ages of deglaciation it is possible to produce a rough estimate of the rate of ice stream retreat through inner Norske Trough (Fig. 9f). Between DA17-092G and PS100-198 the ice stream retreated at approximately 40 m/yr increasing to approximately 62 m/yr through to PS100-270, then increasing again to 125 m/yr across the inner embayment to the present-day coast near the modern ice shelf. The lack of clear glacial depositional features on the seabed in this area (moraines or grounding zone wedges) suggests that ice retreat was continuous during this period. The ice margin then retreated inside of the current margin during the early Holocene. Bennike and Weidick (2001) dated molluscs and whale bones in the vicinity of Blåsø Lake (located near the present day grounding line 70 km from the current ice shelf edge, Fig. 1b) indicating 79N fjord was ice free by *c.* 7.7 ka cal BP. However, recent evidence based on dated molluscs from raised marine deposits around Blåsø Lake (Smith et al., submitted) indicate an earlier ice-free fjord by *c.* 8.5 ka cal BP. Taking the average ^{10}Be age for ice shelf retreat from Bloch Nunatakker

(current ice shelf pinning point) and the recent estimate of 8.5 ka cal BP for ice free conditions at Blåsø Lake provides an estimate of 140 m/yr for retreat of the ice margin through 79N fjord. This is significantly faster than previous estimates of 30–40 m/yr based on ice free conditions around Blåsø Lake by 7.7 ka cal BP (Bennike and Weidick, 2001; Larsen et al., 2018). The trend of increasing retreat rate from *c.* 12 to 8.5 ka cal BP correlates with increasing subsurface ocean temperatures recorded from inner Norske Trough also reaching a peak at *c.* 8.5 ka cal BP (Fig. 9f). While there is no record of how far the ice margin retreated, Smith et al. (2022) record the ice shelf reforming at Blåsø by *c.* 5.3 ka cal BP reaching current thickness by *c.* 4.0 ka cal BP. This is supported by earlier estimates of ice shelf re-growth from *c.* 5.3 ka cal BP (Bennike and Weidick, 2001; Kjær et al., 2022). This advance and reformation of the ice shelf through 79N fjord coincides with a period of reduced subsurface ocean temperatures through inner Norske Trough (Fig. 9e and f). This supports a close link between the retreat dynamics of NEGIS and ocean temperature. However, it must be noted that topography and bathymetry could also play a role in ice stream stability and retreat; a shallowing of water depths in the trough or a narrowing of trough width both act to increase flow resistance impacting on the rate of ice stream retreat (cf. Briner et al., 2009; Jamieson et al., 2012). Notwithstanding the potential role of topography the reconstructions presented here showing surface and subsurface ocean conditions matching the peak in warm conditions during the Holocene suggests the current ice shelf is susceptible to rapid collapse in the near future.

6. Conclusions

A wide-ranging multiproxy study comprising several microfossil groups (benthic and planktic foraminifera, dinocysts, diatoms), geochemistry (stable isotopes, sea ice biomarkers) and sedimentological analysis from a spliced gravity and box core, PS100-198, illustrates the interaction between NEGIS, ocean circulation and sea ice cover during deglaciation and the Holocene on the inner Northeast Greenland continental shelf.

1. The basal age of *c.* 10.9 (range 10.6–11.5) ka cal BP) from rapidly deposited laminated sediments in a proximal glaciomarine environment provides a limiting age on deglaciation at this core site. Proximal glaciomarine conditions persisted below heavy sea ice or potentially an ice shelf until *c.* 10 ka cal BP, but relatively warm Atlantic Water, the RAC, was present at the core site throughout this period.
2. During the early Holocene (10–9 ka cal BP) reducing sedimentation rates and a change from well laminated to diffusely laminated and bioturbated sediments marks a transition to more distal glaciomarine conditions. This coincides with an increase in RAC flow and warming subsurface ocean temperatures, however, heavy sea-ice cover is still likely to dominate surface conditions.
3. From 9 to 7 ka cal BP sedimentation rates continue to reduce as sediments become bioturbated and massive. This coincides with the warmest subsurface water temperatures through the record but continued harsh surface conditions with heavy sea-ice cover indicating strong stratification likely the result of high meltwater flux to the area.
4. During the mid-to late Holocene (7–2 ka cal BP) sedimentation rates remain very low and subsurface ocean conditions cool significantly. There is a continued anti-phase relationship between surface and sub-surface conditions as surface water proxies indicate a shift from relatively heavy to seasonal sea-ice cover.
5. During the late Holocene from 2 ka cal BP there is a shift to an in-phase relationship between surface and subsurface conditions as subsurface waters start to warm again with continued seasonal sea ice conditions and potentially an increase in open water. This becomes more pronounced over the last *c.* 100 years as surface conditions indicate lowest sea ice concentration over the last *c.* 9 ka and subsurface conditions are as warm as the peak during the early Holocene.
6. Based on a comparison with other records in the region there appears to be a close connection between MTOG retreat/dynamics and subsurface ocean temperatures in this region of northeast Greenland. Current subsurface and surface conditions are similar or even more ameliorated in comparison to the early Holocene, the last time the ice shelf within the 79N fjord disintegrated. This indicates the current ice shelf is likely to be highly susceptible to disintegration in the near future.

Author contributions

J.M. Lloyd: Writing – original draft, Writing – review & editing, Conceptualization, Investigation, Methodology, Formal analysis, Visualization, Data curation, Funding acquisition. **S. Ribeiro**: Writing – review & editing, Methodology, Investigation, Formal analysis, Resources. **K. Weckström**: Writing – review & editing, Methodology, Investigation, Formal analysis. Resources. L. Callard: Writing – review & editing, Investigation (Cruise Participation), Visualization. **C. O'Cofaigh**: Writing – review & editing, Conceptualisation, Investigation (Cruise Participation), Funding acquisition. **M. Leng**: Review and Editing, Methodology, Investigation, Resources. **P. Gulliver**: Formal analysis (radiocarbon dating). **D.H. Roberts**: Review and Editing, Conceptualisation, Investigation (Cruise lead), Funding acquisition.

Declaration of competing interest

The authors declare that they have no known competing financial interests or personal relationships that could have appeared to influence the work reported in this paper.

Data availability

The datasets used in this paper are available at the UK NERC Polar Data Centre (http://www.bas.ac.uk/data/uk-pdc/).

Acknowledgements

We thank Captains Schwarze and Wunderlich and the crew of RV Polarstern (cruises PS100 and PS109) for excellent support and cooperation during both cruises. We thank Torsten Kanzow (Chief Scientist on cruises PS100 and PS109) for help and support during the both cruises. We thank AWI for support with radiocarbon dating of small samples using the AWI MICADAS system. We gratefully acknowledge support from AWI for ship time via grants AWI_PS100_01 and AWI_PS109_03. Guillaume Massé and Caroline Guilmette are kindly thanked for the IP25 data. This work was funded by NERC Standard Grant NE/N011228/1. Additional support was provided through the NERC National Environmental Isotope Facility for stable isotope analyses (grant IP-1816-0618, analyses performed by Hilary Sloane, BGS) and NERC Radiocarbon Facility NRCF010001 (allocation number 2113.0418). We acknowledge expertise of Dr Xiaomei Xu performing measurements at the KECK Carbon Cycle AMS Facility, University of California. SR received financial support from the Independent Research Council Denmark (grant nr. 9064-00039B) and KW from Arctic Avenue (spearhead

research project between the University of Helsinki and Stockholm University).

Appendix A. Supplementary data

Supplementary data to this article can be found online at https://doi.org/10.1016/j.quascirev.2023.108068.

References

An, L., Rignot, E., Wood, M., Willis, J.K., Mouginot, J., Khan, S.A., 2021. Ocean melting of the Zachariae Isstrøm and nioghalvfjerdsfjorden glaciers, northeast Greenland. Proc. Natl. Acad. Sci. USA 118, e2015483118. https://doi.org/10.1073/pnas.2015483118.

Arndt, J.E., Jokat, W., Dorschel, B., 2017. The last glaciation and deglaciation of the Northeast Greenland continental shelf revealed by hydro-acoustic data. Quat. Sci. Rev. 160, 45–56. https://doi.org/10.1016/j.quascirev.2017.01.018.

Arndt, J.E., Jokat, W., Dorschel, B., Myklebust, R., Dowdeswell, J.A., Evans, J., 2015. A new bathymetry of the Northeast Greenland continental shelf: constraints on glacial and other processes. G-cubed 16, 3733–3753. https://doi.org/10.1002/2015GC005931.

Battarbee, R.W., 1986. Diatom analysis. In: Berglund, B.E. (Ed.), Handbook of Holocene Palaeoecology and Palaeohydrology. Wiley, Chichester, pp. 527–570.

Belt, S.T., Massé, G., Rowland, S.J., Poulin, M., Michel, C., LeBlanc, B., 2007. A novel chemical fossil of palaeo sea ice: IP25. Org. Geochem. 38 (1), 16–27. https://doi.org/10.1016/j.orggeochem.2006.09.013.

Belt, S.T., Müller, J., 2013. The Arctic sea ice biomarker IP25: a review of current understanding, recommendations for future research and applications in palaeo sea ice reconstructions. Quat. Sci. Rev. 79, 9–25. https://doi.org/10.1016/j.quascirev.2012.12.001.

Belt, S.T., Smik, L., Köseoglu, D., Knies, J., Husum, K., 2019. A novel biomarker-based proxy for the spring phytoplankton bloom in Arctic and sub-arctic settings – HBI T25. Earth Planet Sci. Lett. 523, 115703.

Bennike, O., Bjorck, S., 2002. Chronology of the last recession of the Greenland icesheet. J. Quat. Sci. 17, 211–219. https://doi.org/10.1002/jqs.670.

Bennike, O., Weidick, A., 2001. Late quaternary history around nioghalvfjerdsfjorden and jokelbugten, north-east Greenland. Boreas 30, 205–227.

Blaauw, M., Christen, J.A., 2011. Flexible paleoclimate age-depth models using an autoregressive gamma process. Bayesian Analysis 6 (3), 457–474. https://doi.org/10.1214/11-BA618.

Briner, J.P., Bini, A.C., Anderson, R.S., 2009. Rapid early Holocene retreat of a Laurentide outlet glacier through an Arctic fjord. Nat. Geosci. 2, 496–499. https://doi.org/10.1038/ngeo556.

Budéus, G., Schneider, W., 1995. On the hydrography of the Northeast water polynya. J. Geophys. Res. 100 (C3), 4287–4299. https://doi.org/10.1029/94JC02024.

Budéus, G., Schneider, W., Kattner, G., 1997. Distribution and exchange of water masses in the Northeast Water polynya (Greenland Sea). J. Mar. Syst. 10 (1-4), 123–138. https://doi.org/10.1016/S0924-7963(96)00074-7.

Buizert, C., Keisling, B.A., Box, J.E., He, F., Carlson, A.E., Sinclair, G., DeConto, R.M., 2018. Greenland-wide seasonal temperatures during the last deglaciation. Geophys. Res. Lett. 45, 1905–1914. https://doi.org/10.1002/2017GL075601.

Cage, A.G., Pienkowski, A.J., Jennings, A., Knudsen, K.L., Seidenkrantz, M.-S., 2021. Comparative analysis of six common foraminiferal species of the genera Cassidulina, Paracassidulina, and Islandiella from the Arctic/North Atlantic domain. J. Micropalaeontol. 40, 37–60. https://doi.org/10.5194/jm-40-37-2021.

Catania, G.A., A Stearns, L., Moon, T., Enderlin, E., Jackson, R.H., 2020. Future evolution of Greenland's marine-terminating outlet glaciers. J. Geophys. Res.: Earth Surf. 125, e2018JF004873. https://doi.org/10.1029/2018JF004873.

Corliss, B.H., 1991. Morphology and microhabitat preferences of benthic foraminifera from the northwest Atlantic Ocean. Mar. Micropaleontol. 17, 195–236.

Cowton, T.R., Sole, A.J., Nienow, P.W., Slater, D.A., Christoffersen, P., 2018. Linear response of east Greenland's tidewater glaciers to ocean/atmosphere warming. Proc. Natl. Acad. Sci. USA 115 (31), 7907–7912.

Dai, A., Luo, D., Song, M., Liu, J., 2019. Arctic amplification is caused by sea-ice loss under increasing CO_2. Nat. Commun. 10 (1), 121. https://doi.org/10.1038/s41467-018-07954-9.

Davies, J., Møller Mathiasen, A., Kristiansen, K., Hansen, K.E., Wacker, L., Olsen Alstrup, A.K., Munk, A.L., Pearce, C., Seidenkrantz, M.-S., 2022. Linkages between ocean circulation and the Northeast Greenland ice stream in the early Holocene. Quat. Sci. Rev. 286, 107530. https://doi.org/10.1016/j.quascirev.2022.107530.

de Vernal, A., Radi, T., Zaragosi, S., Van Nieuwenhove, N., Rochon, A., Allan, E., De Schepper, S., et al., 2020. Distribution of common modern dinoflagellate cyst taxa in surface sediments of the Northern Hemisphere in relation to environmental parameters: the new n = 1968 database. Mar. Micropaleontol. 159, 101796. https://doi.org/10.1016/j.marmicro.2019.101796.

Ehrmann, W.U., Thiede, J., 1985. History of mesozoic and cenozoic sediment fluxes to the North Atlantic Ocean. Contrib. Sediment Geol. 15.

Evans, J., Cofaigh, C._O., Dowdeswell, J.A., Wadhams, P., 2009. Marine geophysical evidence for former expansion and flow of the Greenland Ice Sheet across the north-east Greenland continental shelf. J. Quat. Sci. 24, 279–293. https://doi.org/10.1002/jqs.1231.

Fahrner, Dlea, J., Brough, S., Mair, D.W.F., Abermann, J., 2021. Linear response of the Greenland ice sheet's tidewater glacier terminus positions to climate. J. Glaciol. 67 (262), 193–203. https://doi.org/10.1017/jog.2021.13.

Gooday, A.J., Hughes, J.A., 2002. Foraminifera associated with phytodetritus deposits at a bathyal site in the northern Rockall Trough (NE Atlantic): seasonal contrasts and a comparison of stained and dead assemblages. Mar. Micropaleontol. 46, 83–110.

Hanna, E., Cappelen, J., Fettweis, X., Mernild, S.H., Mote, T.L., Mottram, R., Steffen, K., Ballinger, T.J., Hall, R., 2021. Greenland surface air temperature changes from 1981 to 2019 and implications for ice-sheet melt and mass-balance change. Int. J. Climatol. 41, E1336–E1352.

Hansen, K.E., Lorenzen, J., Davies, J., Wacker, L., Pearce, C., Seidenkrantz, M.-S., 2022. Deglacial to Mid Holocene environmental conditions on the northeastern Greenland shelf, western Fram Strait. Quat. Sci. Rev. 293, 107704. https://doi.org/10.1016/j.quascirev.2022.107704.

Hald, M., Korsun, S., 1997. Distribution of modern benthic foraminifera from fjords of Svalbard, European Arctic. J. Foraminifer. Res. 27, 101–122. https://doi.org/10.2113/gsjfr.27.2.101.

Head, M.J., Harland, R., Matthiessen, J., 2001. Cold marine indicators of the late Quaternary: the new dinoflagellate cyst genus Islandinium and related morphotypes. J. Quat. Sci. 16, 621–636.

Heaton, T.J., K€ohler, P., Butzin, M., Bard, E., Reimer, R.W., Austin, W.E.N., Bronk Ramsey, C., Grootes, P.M., Hughen, K.A., Kromer, B., Reimer, P.J., Adkins, J., Burke, A., Cook, M.S., Olsen, J., Skinner, L.C., 2020. Marine20 - the marine radiocarbon age calibration curve (0-55,000 cal BP). Radiocarbon 62, 779–820. https://doi.org/10.1017/RDC.2020.68.

Hopkins, T.S., 1991. The GIN Sea - a synthesis of its physical oceanography and literature review 1972 - 1985. Earth Sci. Rev. 30, 175e318. https://doi.org/10.1016/0012-8252(91)90001-V.

Hughes, N.E., Wilkinson, J.P., Wadhams, P., 2011. Multi-satellite sensor analysis of fast-ice development in the Norske Øer ice barrier, Northeast Greenland. Ann. Glaciol. 52 (57), 151–160. https://doi.org/10.3189/172756411795931633.

Jamieson, S.S.R., Vieli, A., Livingstone, S.J., Cofaigh, C., Stokes, C., Hillenbrand, C.-D., Dowdeswell, J.A., 2012. Icestream stability on a reverse bed slope. Nat. Geosci. 5, 799–802. https://doi.org/10.1038/ngeo1600.

Jennings, A.E., Helgadottir, G., 1994. Foraminiferal assemblages from the fjords and shelf of eastern Greenland. J. Foraminifer. Res. 24, 123–144. https://doi.org/10.2113/gsjfr.24.2.123.

Jennings, A.E., Weiner, N.J., Helgadottir, G., Andrews, J.T., 2004. Modern foraminiferal faunas of the southwestern to northern Iceland shelf: oceanographic and environmental controls. J. Foraminifer. Res. 34, 180–207. https://doi.org/10.2113/34.3.180.

Jennings, A., Andrews, J., Reilly, B., Walczak, M., Jakobsson, M., Mix, A., Stoner, J., Nicholls, K.W., Cheseby, M., 2020b. Modern foraminiferal assemblages in northern Nares Strait, Petermann fjord, and beneath Petermann ice tongue, NW Greenland. Arctic Antarct. Alpine Res. 52, 491–511. https://doi.org/10.1080/15230430.2020.1806986.

Jennings, A.E., Seidenkrantz, M.-S., Knudsen, K.L., 2020a. *Glomulina oculus*, new calcareous foraminiferal species from the high Arctic: a potential indicator of a nearby marine-terminating glacier. J. Foraminifer. Res. 50 (2), 219–234. https://doi.org/10.2113/gsjfr.52.2.219.

Kanzow, T., 2017. The Expedition PS100 of the Research Vessel POLARSTERN to the Greenland Sea and the Fram Strait in 2016. Reports on Polar and Marine Research. Alfred Wegener Institute for Polar and Marine Research, Bremerhaven, No, p. 705.

Khan, S.A., Kjær, K.H., Bevis, M., Bamber, J.L., Wahr, J., Kjeldsen, K.K., Bjørk, A.A., Korsgaard, N.J., Stearns, L.A., van den Broeke, M.R., Liu, L., Larsen, N.K., Muresan, I.S., 2014. Sustained mass loss of the northeast Greenland ice sheet triggered by regional warming. Nat. Clim. Change 4, 292–299. https://doi.org/10.1038/nclimate2161.

Kjær, K.H., Bjørk, A.A., Kjeldsen, K.K., Hansen, E.S., Andresen, C.S., Siggaard-Andersen, M.-L., Khan, S.A., Søndergaard, A.S., Colgan, W., Schomacker, A., Woodroffe, S., Funder, S., Rouillard, A., Jensen, J.F., Larsen, N.K., 2022. Glacier response to the little ice age during the neoglacial cooling in Greenland. Earth Sci. Rev. 227, 103984. https://doi.org/10.1016/j.earscirev.2022.103984.

Knudsen, K.L., Jiang, H., Jansen, E., Eiríksson, J., Heinemeier, J., Seidenkrantz, M.-S., 2004. Environmental changes off North Iceland during the deglaciation and the Holocene: foraminifera, diatoms and stable isotopes. Mar. Micropaleontol. 50, 273–305. https://doi.org/10.1016/S0377-8398(03)00075-6.

Knudsen, K.L., Seidenkrantz, M.S., 1994. Stainforthia feylingi new species from arctic to subarctic environments, previously recorded as Stainforthia schreibersiana (Czjzek). In: Sejrup, H.P., Knudsen, K.L. (Eds.), Late Cenozoic Benthic Foraminifera: Taxonomy, Ecology, and Stratigraphy.Cushman Foundation for Foraminiferal Research, Special Publication, vol. 32, pp. 5–13.

Kochtitzky, W., Copland, L., 2022. Retreat of northern hemisphere marine-terminating glaciers, 2000– 2020. Geophys. Res. Lett. 49, e2021GL096501. https://doi.org/10.1029/2021GL096501.

Korsun, S., Hald, M., 2000. Seasonal dynamics of benthic foraminifera in a glacially fed fjord off Svalbard, European Arctic. J. Foraminifer. Res. 30, 251–271.

Larsen, N.K., Levy, L.B., Carlson, A.E., Buizert, C., Olsen, J., Strunk, A., Bjørk, A.A., Skov, D.S., 2018. Instability of the Northeast Greenland ice stream over the last 45,000 years. Nat. Commun. 9, 1872. https://doi.org/10.1038/s41467-018-04312-7.

Lindeman, M.R., Straneo, F., Wilson, N.J., Toole, J.M., Krishfield, R.A., Beaird, N.L., 2020. Ocean circulation and variability beneath Nioghalvfjerdsbræ (79 North

Glacier) ice tongue. J. Geophys. Res.: Oceans 125, e2020JC016091. https://doi.org/10.1029/2020JC016091.
Lloyd, J.M., 2006. Modern distribution of benthic foraminifera from Disko Bugt, west Greenland. J. Foraminifer. Res. 36, 315–331. https://doi.org/10.2113/gsjfr.36.4.315.
Mayer, C., Schaffer, J., Hattermann, T., Floricioiu, D., Krieger, L., Dodd, P.A., Kanzow, T., Licciulli, C., Schannwell, C., 2018. Large ice loss variability at Nioghalvfjerdsfjorden Glacier, northeast-Greenland. Nat. Commun. 9, 2768. https://doi.org/10.1038/s41467-018-05180-x.
Mertens, K., Verhoeven, K., et al., 2009. Determining the absolute abundance of dinoflagellate cycts in recent marine sediments: the *Lycopodium* marker-grain method put to the test. Rev. Palaeobot. Palynol. 157, 238–252.
Moros, M., Lloyd, J.M., Perner, K., Krawczyk, D., Blanz, T., Kuijpers, A., Jennings, A.E., Witkowski, A., Schneider, R., Jansen, E., 2016. Surface and sub-surface multiproxy reconstruction of mid to late Holocene palaeoceanographic changes in Disko Bugt, West Greenland. Quat. Sci. Rev. 132, 146–160. https://doi.org/10.1016/j.quascirev.2015.11.017.
Mouginot, J., Rignot, E., Scheuchl, B., Fenty, I., Khazendar, A., Morlighem, M., Buzzi, A., Paden, J., 2015. Fast retreat of zachariæ Isstrøm, northeast Greenland. Science 350, 1357–1361. https://doi.org/10.1126/science.aac7111.
Mouginot, J., Rignot, E.J., Bjørk, A.A., van den Broeke, M.R., Millan, R., Morlighem, M., et al., 2019. Forty-six years of Greenland Ice Sheet mass balance from 1972 to 2018. Proc. Natl. Acad. Sci. USA 116 (19), 9239–9244. https://doi.org/10.7280/D1MM37.
Notz, D., Stroeve, J., 2016. Observed Arctic sea-ice loss directly follows anthropogenic CO_2 emission. Science 354 (6313), 747–750. https://doi.org/10.1126/science.aag2345.
O Cofaigh, C., Dowdeswell, J.A., 2001. Laminated sediments in glacimarine environments: diagnostic criteria for their interpretation. Quat. Sci. Rev. 20, 1411–1436. https://doi.org/10.1016/S0277-3791(00)00177-3.
Pados, T., Spielhagen, R.F., Bauch, D., 2015. Oxygen and carbon isotope composition of modern planktic foraminifera and near-surface waters in the Fram Strait (Arctic Ocean) - a case study. Biogeosciences 12, 1733–1752.
Pados-Dibattista, T., Pearce, C., Detlef, H., Bendtsen, J., Seidenkrantz, M.S., 2022. Holocene palaeoceanography of the Northeast Greenland shelf. Clim. Past 18, 103–127.
Patterson, R.T., Guilbault, J.-P., Thomson, R.E., 2000. Oxygen level control on foraminiferal distribution in effingham inlet, vancouver island, British columbia, Canada. J. Foraminifer. Res. 30, 321–335.
Polyak, L., Korsun, S., Febo, L.A., Stanovoy, V., Khusid, T., Hald, M., Paulsen, B.E., Lubinski, D.J., 2002. Benthic foraminiferal assemblages from the southern Kara Sea, a river-influenced Arctic marine environment. J. Foraminifer. Res. 32, 252–273. https://doi.org/10.2113/32.3.252.
Polyakov, I., Pnyushkov, A., Alkire, M., Ashik, I., Baumann, T., Carmack, E., Goszczko, I., Guthrie, J., Ivanov, V., Kanzow, T., Krishfield, R., Kwok, R., Sundfjord, A., Morison, J., Rember, R., Yulin, A., 2017. Greater role for atlantic inflows on sea-ice loss in the eurasian basin of the Arctic Ocean. Science 356, 285–291.
Rasmussen, T.L., Pearce, C., Andresen, K.J., Nielsen, T., Seidenkrantz, M.-S., 2022. Northeast Greenland:ice-free shelf edge at 79.4°N around the Last Glacial Maximum 25.5–17.5 ka. Boreas 51, 759–775. https://doi.org/10.1111/bor.12593.
Reeh, N., Thomsen, H.H., Higgins, A.K., Weidick, A., 2001. Sea ice and the stability of north and northeast Greenland floating glaciers. Ann. Glaciol. 33, 474–480. https://doi.org/10.3189/17275.640178181554.
Rignot, E.J., Kanagaratnam, P., 2006. Changes in the velocity structure of the Greenland ice sheet. Science 311, 986–990. https://doi.org/10.1126/science.1121381.
Rochon, A., de Vernal, A., Turon, J.L., Matthiessen, J., Head, M.J., 1999. Distribution of recent dinoflagellate cysts in surface sediments from the North Atlantic Ocean and adjacent seas in relation to sea-surface parameters. Am. Assoc. Stratigr. Palynol. Contrib. Ser. 35, 1–146.
Schaffer, J., Appen, W.-J. von, Dodd, P.A., Hofstede, C., Mayer, C., Steur, L. de, Kanzow, T., 2017. Warm water pathways toward Nioghalvfjerdsfjorden Glacier, northeast Greenland. J. Geophys. Res.: Oceans 122, 4004–4020. https://doi.org/10.1002/2016JC012462.
Schaffer, J., Kanzow, T., von Appen, W.-J., von Albedyll, L., Arndt, J.E., Roberts, D.H., 2020. Bathymetry constrains ocean heat supply to Greenland's largest glacier tongue. Nat. Geosci. 13, 227–231.
Schroder-Adams, C.J., Cole, F.E., Medioli, F.S., Mudie, P.J., Scott, D.B., Dobbin, L., 1990. Recent Arctic shelf foraminifera: seasonally ice-covered areas vs. perennially ice-covered areas. J. Foraminifer. Res. 20, 8–36.
Seidenkrantz, M.-S., 2013. Benthic foraminifera as palaeo sea-ice indicators in the subarctic realm: examples from the Labrador Sea-Baffin Bay region. Quat. Sci. Rev. 79, 135–144. https://doi.org/10.1016/j.quascirev.2013.03.014.
Sejr, M., Stedmon, C., Bendtsen, J., Abermann, J., Juul-Pedersen, T., Mortensen, J., Rysgaard, S., 2017. Evidence of local and regional freshening of the Northeast Greenland coastal waters. Sci. Rep. 7, 13183. https://doi.org/10.1038/s41598-017-10610-9.
Shepherd, A., Ivins, E., Rignot, E., Smith, B., van den Broeke, M., Velicogna, I., Whitehouse, P., Briggs, K., Joughin, I., Krinner, G., Nowicki, S., Payne, T., Scambos, T., Schlegel, N., G, A., Agosta, C., Ahlstrøm, A., Babonis, G., Barletta, V.R., Bjørk, A.A., Blazquez, A., Bonin, J., Colgan, W., Csatho, B., Cullather, R., Engdahl, M.E., Felikson, D., Fettweis, X., Forsberg, R., Hogg, A.E., Gallee, H., Gardner, A., Gilbert, L., Gourmelen, N., Groh, A., Gunter, B., Hanna, E., Harig, C., Helm, V., Horvath, A., Horwath, M., Khan, S., Kjeldsen, K.K., Konrad, H., Langen, P.L., Lecavalier, B., Loomis, B., Luthcke, S., McMillan, M., Melini, D., Mernild, S., Mohajerani, Y., Moore, P., Mottram, R., Mouginot, J., Moyano, G., Muir, A., Nagler, T., Nield, G., Nilsson, J., No€el, B., Otosaka, I., Pattle, M.E., Peltier, W.R., Pie, N., Rietbroek, R., Rott, H., Sandberg Sørensen, L., Sasgen, I., Save, H., Scheuchl, B., Schrama, E., Schr€oder, L., Seo, K.-W., Simonsen, S.B., Slater, T., Spada, G., Sutterley, T., Talpe, M., Tarasov, L., van de Berg, W.J., van der Wal, W., van Wessem, M., Vishwakarma, B.D., Wiese, D., Wilton, D., Wagner, T., Wouters, B., Wuite, J., 2020. Mass balance of the Greenland ice sheet from 1992 to 2018. Nature 579, 233–239.
Smith, J.A., Callard, L., Bentley, M.J., Jamieson, S.S.R., Sánchez-Montes, M.L., Lane, T.P., Lloyd, J.M., McClymont, E.L., Darvill, C.M., Rea, B.R., O'Cofaigh, C., Gulliver, P., Ehrmann, W., Jones, R.S., Roberts, D.H., 2022. Holocene history of 79° N ice shelf reconstructed from epishelf lake and uplifted glacimarine sediments. Cryosphere Discuss. https://doi.org/10.5194/tc-2022-173 [preprint].
Sneed, W.A., Hamilton, G.S., 2016. Recent changes in the Norske Øer ice barrier, coastal Northeast Greenland. Ann. Glaciol. 57 (73), 47–55. https://doi.org/10.1017/aog.2016.21.
Straneo, F., Heimbach, P., 2013. North Atlantic warming and the retreat of Greenland's outlet glaciers. Nature 504 (7478), 36–43. https://doi.org/10.1038/nature12854.
Straneo, F., Sutherland, D.A., Stearns, L.A., Catania, G.A., Catania, G., Heimbach, P., et al., 2019. The case for a sustained Greenland ice sheet-ocean observing system (GrIOOS). Front. Earth Sci. 6 (138), 391. https://doi.org/10.3389/fmars.2019.00138.
Stuiver, M., Reimer, P.J., Reimer, R.W., 2021. CALIB 8.1 [WWW program] at. http://calib.org.
Syring, N., Lloyd, J.M., Stein, R., Fahl, K., Roberts, D.H., Callard, L., O'Cofaigh, C., 2020. Holocene interactions between glacier retreat, sea ice formation, and Atlantic water advection at the inner Northeast Greenland continental shelf. Paleoceanogr. Paleoclimatol. 35, e2020PA004019. https://doi.org/10.1029/2020PA004019.
van den Broeke, M., Bamber, J., Ettema, J., Rignot, E., Schrama, E., van de Berg, W., van Meijgaard, E., Velicogna, I., Wouters, B., 2009. Partitioning recent Greenland mass loss. Science 326, 984–986.
Wadhams, P., 1981. The ice cover in the Greenland and Norwegian seas. Rev. Geophys. Space Phys. 19 (3), 345–393. https://doi.org/10.1029/RG019i003p00345.
Werner, K., Müller, J., Husum, K., Spielhagen, R.F., Kandiano, E.S., Polyak, L., 2016. Holocene sea subsurface and surface water masses in the Fram Strait – comparisons of temperature and sea-ice reconstructions. Quat. Sci. Rev. 147, 194–209.
Winkelmann, D., Jokat, W., Jensen, L., Schenke, H.-W., 2010. Submarine end moraines on the continental shelf off NE Greenland e implications for Lateglacial dynamics. Quat. Sci. Rev. 29, 1069–1077. https://doi.org/10.1016/j.quascirev.2010.02.002.
Wollenburg, J.E., Mackensen, A., 1998. Living benthic foraminifers from the central Arctic Ocean: faunal composition, standing stock and diversity. Mar. Micropaleontol. 34, 153–185. https://doi.org/10.1016/S0377-8398(98)00007-3.
Yin, J., Overpeck, J.T., Griffies, S.M., Hu, A., Russell, J.L., Stouffer, R.J., 2011. Different magnitudes of projected subsurface ocean warming around Greenland and Antarctica. Nat. Geosci. 4, 524–528.
Zehnich, M., Spielhagen, R.F., Bauch, H.A., Forwick, M., Hass, H.C., Palme, T., Stein, R., Syring, N., 2020. Environmental variability off NE Greenland (western Fram Strait) during the past 10,600 years. Holocene 30 (12), 1752–1766. https://doi.org/10.1177/0959683620950393.
Zonneveld, K.A.F., Marret, F., Versteegh, G.J.M., Bonnet, S., Bouimetarhan, I., Crouch, E., de Vernal, A., et al., 2013. Atlas of modern dinoflagellate cyst distribution based on 2405 datapoints. Rev. Palaeobot. Palynol. 191, 1–197.